Response to Anonymous Referee #1

"This manuscript by Malte Heinemann et al. introduces a new parameterization of the ballasting effect in the MPI-OM/HAMOCC ocean model. This effect, in which sinking dust particles accelerate the soft tissue pump carbon export, has until now not been included in iron fertilization estimates of LGM dust. It is therefore a very welcome development. However, the convoluted (and ethically questionable) way the authors force an iron limited Southern Ocean makes the iron fertilization results very unbelievable."

There seems to be a misunderstanding. We do not force the Southern Ocean to be iron-limited. Quite the contrary - the Southern Ocean in our model study is *not* iron limited because we do use the more recent Mahowald et al. dust forcing from 2006, which is the default in the model version used. The decision to return to the older dust deposition reconstruction temporarily in later HAMOCC versions to achieve a more realistic iron limitation in the Southern Ocean was taken within the HAMOCC development group at the MPI for Meteorology. We do not use these later model versions; we only wanted to clarify that, if one of the later model versions with an iron-limited Southern Ocean is used (in a hypothetical future study by ourselves or somebody else), the simulated ocean CO_2-uptake in response to an iron addition in the Southern Ocean will likely be larger.

We emphasize in the revised manuscript that we did not use the version with the Mahowald et al. (2005) dust deposition rates (Section 5, page 17 lines 5-28 of the revised manuscript; see also response to major comments (1) and (3) below).

In addition, there is no way to estimate the robustness of the ballasting results presented here as there is no sensitivity analysis or uncertainty estimation. For these reasons I cannot support the publication of this manuscript in its current form.

We think that the suggested sensitivity study is beyond the scope of this technical development paper, as detailed below in our response to major comment (1).

Major Comments:
(1) The estimation of the ballasting effect was performed using only the Mahowald et al., 2005 dataset. I guess that for a theoretical study on this effect, any dust flux dataset will do, even an outdated one. But what would have happened if the authors used a different dust flux dataset, would the results have been 20 ppm pCO2 drawdown due to ballasting, or 1 ppm? To get a feel for the uncertainty of the results, the authors should either use several different (and recent!) dust flux datasets, or include a sensitivity analysis (e.g. 2x and 0.5x the Mahowald 2005 dust fluxes).

We agree with the referee that it would be better to use a more recent dust deposition estimate. In fact, we are currently working on the implementation of the recent estimate by Albani et al. (2016), which was unfortunately not yet available at the start of this project. After this implementation, not only the LGM dust sensitivity simulations would have to be re-done, but all the presented simulations, including the model spin-ups with and without ballasting. Changing the dust deposition fields will likely require re-tuning of the cyanobacteria production, it will lead to a different model setup also for the control simulation without ballasting, and require a new model release. As discussed in our general comment to all reviewers, we think that the repetition of our simulations with updated dust fields is therefore beyond the scope of this paper.

Simply scaling the LGM dust anomaly by a factor of 0.5 or 2 would be an easier-to-achieve sensitivity study, but the meaning of the results would be similarly questionable, since the problem of too high iron availability in the control simulation would persist.

(2) Figure 4(a): Even after 4,500 years the iron fertilization has not yet reached an equilibrium state for the atmospheric pCO2. Could you discuss that in chapter 4.4? Is there some long-term ocean feedback?

We extended all sensitivity simulations by another 2000 years, but even after 6500 years the ocean in the LGM iron run keeps taking up more CO_2 than in the reference run with modern dust/iron.

We attribute this long-term trend to a continuously reduced PIC/POC ratio of the export production relative to the reference simulation, and hence a continuously reduced export of alkalinity, while the PIC/POC ratio in the LGM ballast simulation increases again over time due to reduced primary productivity in response to nitrate depletion (Fig. 2 in this response; the anomalous organic matter export flux and the rain ratio anomalies in Fig. 2a and c are now also shown as Fig. 5 d and f in the revised manuscript).

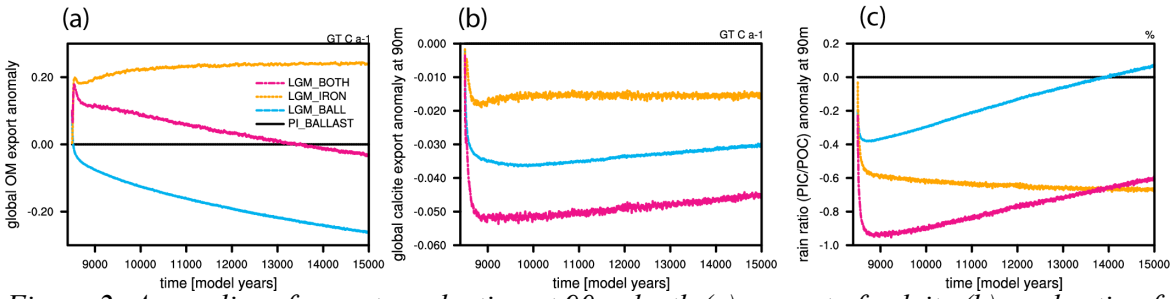

Figure 2: Anomalies of export production at 90m depth (a), export of calcite (b), and ratio of calcite versus organic matter (PIC/POC) for the simulation with LGM dust as ballast (LGM_BALL), with LGM dust for iron fertilization (LGM_IRON), and LGM dust for both (LGM_BOTH).

Note that long-term trends can also arise if the sediment burial fluxes of organic matter, calcite and opal are not balanced by the weathering fluxes – which we did not adjust in the sensitivity simulations.

In the revised manuscript, we added a discussion of both, the role of the PIC/POC changes for the simulated long-term trend, as well as of the potential role of sediment – water column interactions to the corresponding section (now Section 4.2; page 16 lines 14-22).

(3) Page 15, lines 3-10: let me get this straight: Your model doesn't reproduce Southern Ocean iron fertilization using the Mahowald 2006 dust fluxes and you therefore conclude that the Mahowald 2006 dust fluxes are overestimated? And instead of including the updated version of that dataset (Albani et al., 2014), you decide to include data that you like better from an older paper from 2005, which itself is based on old model studies from 2003 and 2004? That is very sketchy. Maybe the model you are using is just bad at reproducing nutrient limitation and shouldn't be used at all for iron fertilization studies? I suggest that the authors either perform the simulations again with up-to-date estimates of dust fluxes using an updated version or a different model, or that they remove any mention of iron fertilization

from the text and only discuss the ballasting effect.

Again, there seems to be a misunderstanding. We did not use the dataset from 2005. We only wanted to point out that, if the older dataset was used, the Southern Ocean would again be iron limited. The Southern Ocean in our model is not iron limited, because we used the relatively newer dust deposition product.

That said, the most recent dataset by Albani et al. (2016) looks more similar to the 2005 data than to the 2006 data (see Fig. 1 in AC1 / general comment to all reviewers).

As discussed in the general comment to all authors, we would rather not remove the iron results, because the cyanobacterial response that leads to the CO_2 drawdown is still at least consistent within the model; although the lack of iron fertilization in the Southern Ocean is not in line with observations.

In the revised manuscript, we clarify that the focus of this study is the introduction of the ballasting parameterization and its effect, and not the iron results. To this end, we changed the title (removed "and iron addition"), modified the abstract (now explicitly mentioning diazotroph and non-diazotroph effects in the last sentence), and explain already in the introduction that the iron effect is likely underestimated, and why we still do look at the iron effect (page 3 lines 8-12).

Minor Comments:
page 11, line 5: There are many black lines in Figure 4.

The sentence was removed / content of this subsection was moved to Section 2.1 (Configuration of MPIOM/HAMOCC).

Page 11, lines 30-31: The authors argue that primary production is reduced over many ocean regions because of nitrate depletion due to increased particle sinking speeds. I would add here that this is important in nitrate-limited zones. In fact, it would be interesting to compare the relative strengths of this effect to the main ballasting effect.

We agree that the effect of nitrate depletion is only important in nitrate-limited zones; however, in our model, the entire surface ocean is nitrate limited (old manuscript, page 14, line 13). Hence, the effect can play a role everywhere. We point this out again in the revised manuscript (page 15, lines 5-7). If any parts of the surface ocean were limited by phosphate, then the accelerated phosphate export due to higher sinking speeds would likely also lead to a reduced primary production in those areas.

Since the "main ballasting effect" is exactly the acceleration of particles, including particulate nitrate, it is unclear to us what is meant by separating the two effects. Did the comment aim at diagnosing the effects in different locations (i.e., nitrate depleted areas only versus other areas), or at performing new simulations, e.g., somehow keeping the NPP or nitrate export constant for the LGM ballasting sensitivity experiment? But then again, the constant NPP will also affect particle ballasting. Maybe the reviewer can elaborate?

Response to Anonymous Referee #2

The manuscript by Heinemann et al., describes the addition of a ballasting parameterisation within the MPI-OM/HAMOCC model and is used to quantify the contribution of ballasting to glacial-interglacial changes in CO_2 associated with changing dust fluxes. The authors find that ballasting by dust particles has a smaller drawdown of atmospheric CO_2 compared with the effect of iron fertilisation when forced with glacial dust fluxes. I think this is a really interesting question to explore as there has been comparatively less focus on processes affecting organic carbon fluxes in the ocean interior than on the effects of iron fertilisation. However, I think it's difficult to reach a satisfying answer because the iron fertilisation effect in these experiments does not occur in the Southern Ocean as generally understood by the iron hypothesis. The authors are open about this in the manuscript but ultimately I think this limits the findings. I have detailed a number of comments on this as well as the ballasting parameterisation and sediment model below. If the authors are able to address this key issue then I think the manuscript would suitable for publication.

Please see responses to the detailed comments below.

General Comments:

The modelled iron fertilisation effect in the model does not occur in the Southern Ocean as understood by the iron hypothesis. This has a number of issues for interpreting the results. Firstly, CO_2 drawdown associated with export production varies by location (DeVries et al., 2012) and therefore the CO_2 sensitivity for the iron fertilisation experiments may not be comparable. The sensitivity falls below the cited range in the introduction (8 ppm vs. 15-40 ppm).

We agree with the reviewer and clarify in the revised manuscript that the presented CO_2 sensitivity for the iron fertilization is not comparable to the range cited in the introduction, because non-diazotrophic phytoplankton is not iron limited anywhere in our control simulations (this is now clarified in the last sentence of the abstract, the last paragraph of the introduction, and in an extended discussion on page 17 lines 5-28 in the revised manuscript). We still think that presenting the iron sensitivity results is interesting enough, illustrating the effect of iron fertilization on cyanobacteria.

In the revised manuscript, the focus was shifted to the ballasting parameterization and effects by more clearly pointing out the iron fertilization limitations, and especially by no longer mentioning the iron effects in the title of the manuscript.

Secondly, changes in ballasting and sinking rates will lead to changes in nutrient distributions which could potentially enhance or reduce any export production changes associated with iron fertilisation. For example, an increase in export production with iron fertilisation may be reduced if ballasting increases sinking speeds locally relocating nutrients within the water column. For these reasons, I think the comparison of CO_2 changes is hard to interpret fully.

We point out in the revised manuscript that, when comparing the effects of iron fertilization and ballasting, potential interactions between the two effects such as in the given example have to be kept in mind. We do find, however, that these effects appear to be small in our experiments; the sum of the ballasting effect and the iron fertilization effect on CO_2 is only

slightly larger than their combined effect on CO_2 (Fig. 3 in this response / now also included as Fig. 5c in the revised manuscript). But we also acknowledge that this may be different for more realistic simulations of the iron fertilization effects in the Southern Ocean (page 17, lines 27-28 in the revised manuscript).

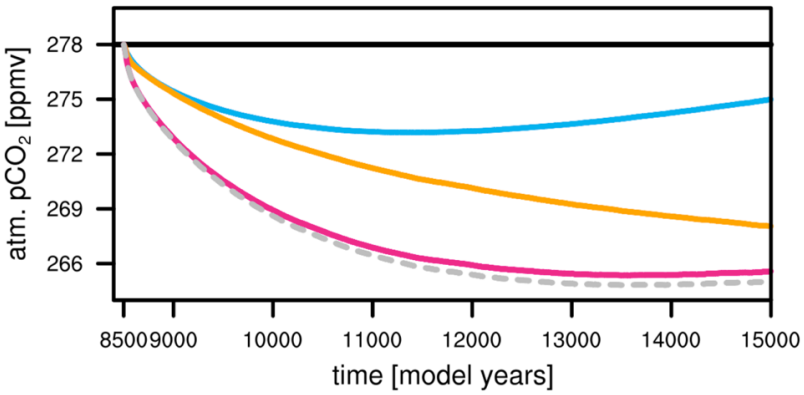

Figure 3: Sum of ballasting effect and iron fertilization effect on atmospheric pCO_2 (grey dashed line) compared to the fertilization effect alone (orange; LGM_IRON), the ballasting effect alone (blue; LGM_BALL), and the combined effect (pink; LGM_BOTH).

The description of the ballasting scheme, its appropriateness and impacts needs better description overall. The scheme from Gehlen et al., (2006) assigns a single sinking rate to all particle types according to the average excess density particles. While this scheme has been used previously, I think a few things need discussion: this scheme assumes a key role for particle aggregation (this is really a ballasting and aggregation parameterisation) and that this scheme differs considerably from other ballasting schemes used previously, (Howard et al., 2006; Hoffman and Schellnhuber 2009).

In the revised manuscript, we include the suggested references and describe the main difference of our / the Gehlen et al. scheme compared to the type of schemes used therein – namely that only a fraction of the POC flux in these schemes is associated with ballast (page 3, lines 19-21). As detailed in the response to your specific comment below (to Pg 7, lines 9-10 / discussion of advantages and disadvantages of the used ballasting scheme), we also discuss the lack of an explicit aggregation scheme (page 3, lines 21-25 in the revised manuscript).

Given the significant impact on opal sinking rates, I think this needs some thought. Additional figures, such as Taylor diagrams showing statistical fits for the new and old scheme versus observations would help assure me this scheme is working well.

We added a Taylor diagram to the revised manuscript, showing statistical fits of nutrient concentrations, including silicate, for both schemes versus World Ocean Atlas data (Fig. 4 here and in the revised manuscript). For silicate, the diagram illustrates that the magnitude of spatial variability of the silicate distribution in the run with ballasting is closer to observations, while the correlation with observations hardly differs (added description / comparison to revised manuscript, page 10 line 17 to page 11 line 2).

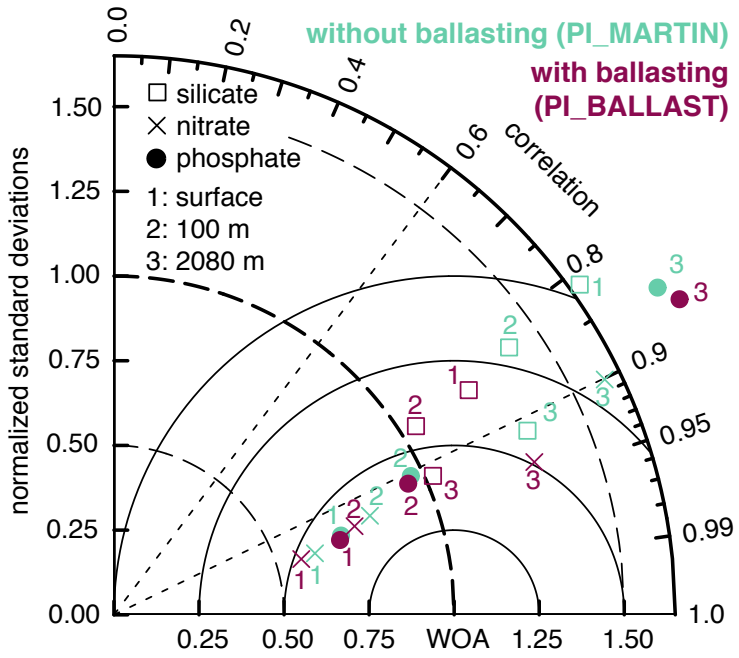

Figure 4: Taylor diagram comparing annual mean silicate (squares), nitrate (crosses), and phosphate concentrations (dots) at 3 different depths (numbers) of the preindustrial reference simulations with Martin-type sinking (MARTIN, aquamarine) and with particle ballasting (BALLAST, pink) to World Ocean Atlas data (WOA; Garcia et al. 2013).

Please also state all the units when describing the ballasting parameterisation.

We added that the mass concentration c_dust is the mass of dust per unit volume of seawater (e.g., in g per cm3 seawater), and that the molar concentrations PSI_b are given in mol C and mol Si per unit volume of seawater respectively (e.g., for PSI_detritus and PSI_calcite in mol C per cm3 seawater).

The inclusion of sediments here is not well described or justified. The experiments don't seem to have reached a steady-state (e.g.,Figure 4a), is this because the sediments are still responding? Depending on the processes in the sediment model, there could be different responses to iron fertilisation and ballasting as ballasting will affect the ratios of particulate matter reaching the seafloor (e.g., Ridgwell 2003). Would it be possible to isolate and quantify the effect of sediments on the CO_2 drawdown?

The standard version of MPIOM/HAMOCC does come with the activated sediment module, which was described briefly in Section 2.3 of Ilyina et al. (2013), or more extensively by Heinze et al. (1999). The reference to the more detailed description of the sediment module (Heinze et al. 1999) was added to the revised manuscript. If it had been easily possible, we would have preferred to first turn off interactions of the ocean column with the sediment to avoid this problem. In future studies, an offline version of the sediment module that was recently developed at the MPI for Meteorology can be used to accelerate this equilibration process (for example to achieve equilibrium for the LGM, before a transient deglaciation simulation is started).

Regarding the long-term trends seen in Fig. 4a of the original manuscript, the strongest trend in atmospheric pCO_2 occurs in the iron fertilization experiment, and we attribute this long-

term trend to a continuously reduced PIC/POC ratio of the export production relative to the reference simulation, and hence a continuously reduced export of alkalinity, while the PIC/POC ratio in the LGM ballast simulation increases again over time due to reduced primary productivity in response to nitrate depletion (see Fig. 2 in our response to Referee #1 / Fig. 5 d and f in the revised manuscript; a discussion of this trend was added on page 16, lines 14-16).

However, it is still possible that changes in the sediment are contributing to the simulated long-term trend, and we discuss this possibility in the revised manuscript. Quantifying this contribution is difficult, because the equilibration time with the sediment is very long, and equilibrium in the sediment has hardly been reached in the presented sensitivity simulations (see, e.g., the positive trend of calcite fluxes into the sediment, Fig. 5b), although we extended all sensitivity runs by another 2000 years. To estimate the potential contribution of sediment—water column interactions to the atmosphere—ocean CO_2 flux anomalies, we analyzed time series of the anomalous total organic carbon and calcite pools in the sediment (not shown). Changes in the anomalous total carbon and calcite pools can be translated directly into changes of the water column pool anomalies, because the prescribed weathering flux inputs are identical between all the simulations.

For LGM_BALL, we find that the organic carbon pool in the sediment grows faster than in the reference run with modern dust for ballasting (PI_BALLAST), potentially contributing to the simulated ocean CO2 uptake. This anomalous organic carbon pool trend amounts to an uptake of about 0.01 Gt C per year by the sediment, which is comparable in magnitude to the atmosphere–ocean CO_2 flux anomalies. Moreover, relative to PI_BALLAST, the sediment calcite pool in LGM_BALL is reduced by about $0.2 \cdot 10^{16}$ mol Ca after the first 3000 years of the sensitivity experiment, which can be translated into a global mean ocean alkalinity increase by ∼3 mmol m^{-3}, also potentially contributing to the simulated ∼10 mmol m^{-3} alkalinty increase in LGM_BALL at the surface.

For LGM_IRON, a slightly reduced calcite pool in the sediment compared to PI_BALLAST may also contribute a small portion to the simulated long term atmospheric pCO_2 drawdown. The sediment calcite pool reduction is equivalent to an alkalinity increase in the water column of less than 2 mmol m^{-3}, compared to a surface alkalinity increase by about 16 mmol m^{-3} after 6500 years in LGM_IRON. Less organic carbon is stored in the sediment in LGM_IRON relative to the reference with modern dust (PI_BALLAST), meaning that the exchange of organic matter between the sediment and the water column does not contribute to the simulated long-term ocean CO_2 uptake in LGM_IRON.

In the revised manuscript, we added a discussion of the potential role of sediment—water column interactions for the LGM dust sensitivity experiments for ballasting (LGM_BALL) and iron fertilization (LGM_IRON) to the corresponding sections (now Section 4.1, page 15, lines 15-25, and Section 4.2, page 16 lines 14-22).

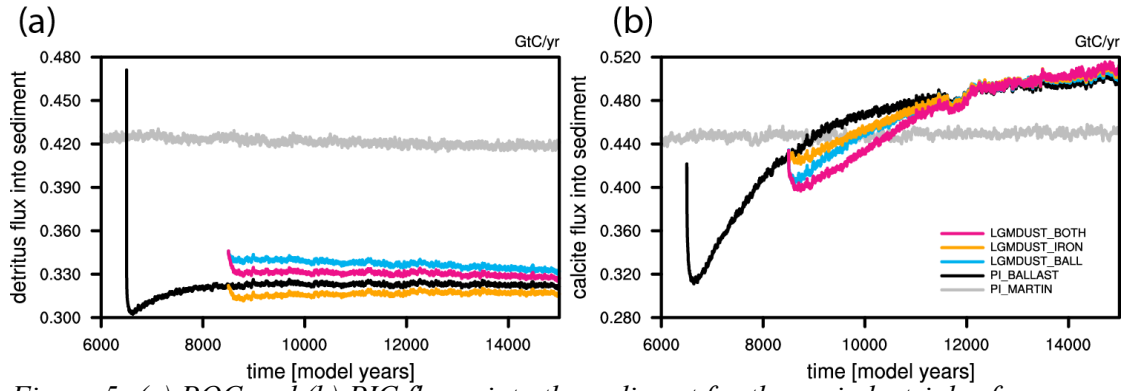

Figure 5: (a) POC and (b) PIC fluxes into the sediment for the preindustrial reference runs with Martin-type sinking (gray) and with particle ballasting (black), as well as for the LGM dust sensitivity experiments using the dust only for ballasting (blue; LGM_BALL), only for iron fertilization (orange; LGM_IRON), and for both (pink; LGM_BOTH).

Specific Comments:

Pg 2, lines 20 - 30: The citations for dust/lithogenic ballasting seem limited to only a few papers (Klaas and Archer 2002; Dunne et al., 2007) with a lack of more recent papers focussing on observed effects.
We added van der Jagt et al. 2018 to the reference list.

Pg 3, line 14: I am not sure the experiments here can be called equilibrium experiments as atmospheric CO_2 still seems to be changing in Figure 4a, and as also mentioned at the bottom of page 5.
Agreed. The word "equilibrium" was deleted.

Pg 3, line 33: The description of the box model of atmospheric CO_2 referred to here is quite limited. The description later on might be better located here.
The content of Section 4.2 was moved here (now page 4, lines 13-30).

Pg 4, lines 3-5: This is quite a lot of description of the grid-setup, does it have implications or relevance for the interpretation of the results?
The model grid-setup needs to be at least mentioned, since several pre-defined MPIOM grid setups exist. Some model parameters are set according to the resolution – for example the primary production depends on the thicknesses of the top layers (because growth rates are computed using the insolation at the top of each box). We shortened the description in the revised manuscript a bit / as far as we think is reasonable.

Figure 2: It might be helpful to also see the global flux profile, e.g., a Martin Curve equivalent, to get a handle on how the sinking speeds contribute to changes in particulate fluxes.
A Martin-curve-equivalent was added in the revised manuscript, illustrating that the global fluxes are enhanced above 2000m depth by the higher mean sinking speed in the simulation with ballasting (Fig. 6 here / Fig. 2a in the revised manuscript).

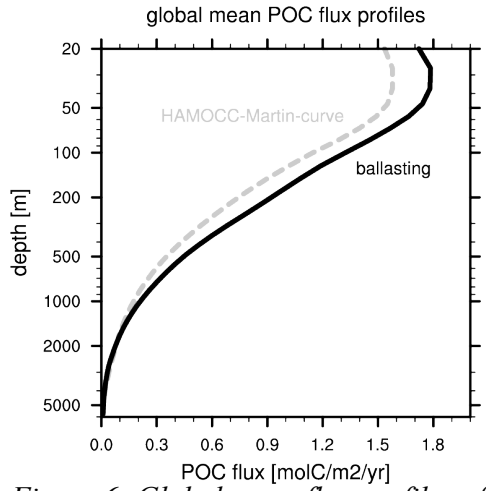

Figure 6: Global mean flux profiles of particulate organic carbon for the modern control simulation with Martin-type sinking (gray dashed) and the simulation with particle ballasting (black).

Pg 7, lines 9-10: a change in the sinking rate for opal from 30 m day^{-1} to 5 m day^{-1} is quite dramatic. I would like some discussion about this change, e.g., how does it compare to values in literature and other models? Is this scheme better because of the explicit use of density or are there other things missing? Adding some summary plots about different tracers (see general comments) would also help clarify the impact of this change.

We discuss the advantages and potential disadvantages or improvements of the ballasting scheme in more detail in the revised manuscript. The explicit calculation of the excess density allows us to test the ballasting hypothesis. As already mentioned in the original manuscript, one potential improvement would be the inclusion of aggregate porosity (in the revised manuscript, this is found in the paragraph starting on page 17 line 34).
Following your general comment above, we highlight in the revised manuscript that the ballasting parameterization is implicitly also an aggregation model (page 3, lines 21-25), which assumes instant formation of aggregates with the computed density, neglecting the complex biological and physical aggregation and disaggregation processes that occur in reality (e.g., Lam and Marchal 2015) or that are explicitly captured in more complex (and computationally more expensive) aggregation models (e.g., Kriest and Evans 2000). Moreover, no aggregate sizes, size distributions or particle shapes are being computed in our ballasting parameterization, and hence potential effects of aggregate size distribution or shape changes on sinking velocities are neglected (see, e.g., Komar et al., 1981, for sinking speeds of approximately cylindrical fecal pellets). We added this point to the discussion in the revised manuscript (page 18, lines 5-7).

We would like to emphasize that the reduction of the opal sinking speed from the prescribed value of 30m/day to about 5m/day (as opal sinking within the virtual aggregates) only occurs in the euphotic zone. The sinking speed increases with depth to about 20m/day at 1km depth, to 30m/day at 3km, and to as much as 120m/day below 5km depth (within the virtual aggregate; black curve in Fig. 2b in the revised manuscript). Still, the sinking speeds are small compared to, e.g., those in the ocean biogeochemical model PISCES-v2 (Aumont et al., 2015), where the speed increases from about 50m/day at the surface to about 240m/day close to 5km depth. However, also the opal dissolution rates differ between the models, with a more complex formulation in PISCES depending on temperature and saturation states, resulting in rates up to 0.025 day^{-1}, which is 2.5 times faster than the standard remineralization in HAMOCC, and 15 times faster than the rate used in our simulations with

ballasting. The better fit to observations of the simulated silicate concentrations in our simulations with ballasting compared to the standard version of HAMOCC suggests that the ballasting parameterization is an improvement over the standard opal sinking and remineralization parameterization (see Taylor-diagram above).

Pg 8, lines 15-20: no quantification of opal export here
Opal production (Fig. 1e in the manuscript) and opal export at 90m (not shown) are reduced by about 30 % in the simulation with modern dust and ballasting compared to the run without ballasting (production 76 versus 108 Tmol Si yr^{-1}, export 72 versus 103 Tmol Si yr^{-1}). We added those numbers to the revised manuscript.

Pg 8, lines 26-29: As I understand, the sediment trap data presented in Honjo et al., (2008) is normalised to 2000 m using the Martin curve on the basis that gravitational settling is the dominant process at this depth. The data here is reported at 1000 m. Did you apply the same normalisation and if so can the same assumptions apply at this depth?

Indeed, we accidentally compared the data to the simulated 960m export instead of to the simulated export close to 2000m depth. We corrected our mistake (Figure 7 below), now comparing the transfer efficiency from Honjo et al. (export at 2000m depth divided by export at 100m depth) to the simulated transfer efficiency computed from the fluxes at 2080m and 100m depth. The simulated transfer efficiencies match the data from Honjo et al. much better now; the mistake explains why we previously overestimated the transfer efficiency. We corrected Fig. 3 and its caption in the revised manuscript accordingly.

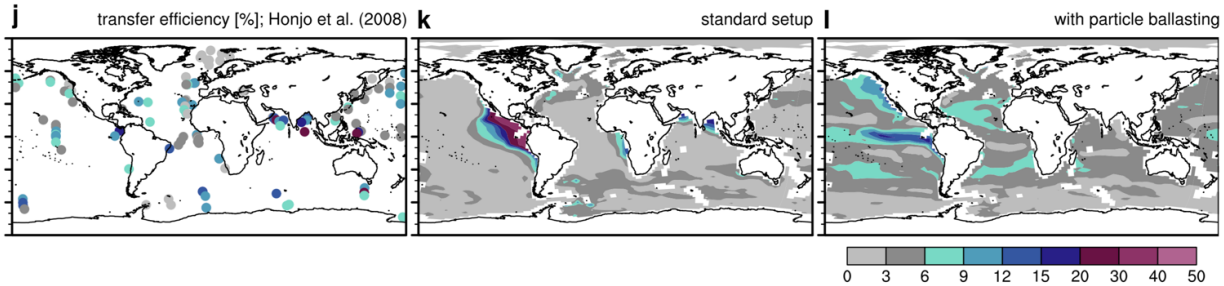

Figure 7: New Fig. 3 j-l. Transfer efficiency computed from Honjo et al. (2008, panel j), compared to the simulated transfer efficiencies in the control run with Martin-type sinking (k) and the run with ballasting and modern dust deposition (l) computed as the fraction of detritus export at 2080m compared to 100m depth.

Figure 3: What causes the transfer efficiency pattern in the standard model (panel k)? From the previous description, it seems like this should be globally uniform.

The pattern arises because detritus remineralization rates depend on oxygen availability. Denitrification and sulfate reduction remineralization rates combined are lower than aerobic remineralization rates (see Eq. 6 of Ilyina et al., 2013), leading to higher transfer efficiencies in oxygen minimum zones (Figure 8 and Figure 7 / new Fig. 3k in the revised manuscript). In the simulations with particle ballasting, this effect of lower remineralization rates in oxygen minimum zones is partly compensated by reduced ballasting by calcite due to the corrosive waters, resulting in lower settling speeds and transfer efficiencies in the OMZs (Figure 7 / new Fig. 3l in the revised manuscript).

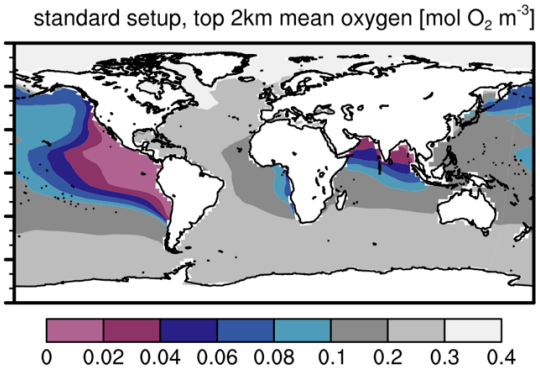

Figure 8: Mean oxygen concentration in the upper 2km of the water column in the modern control simulation without ballasting.

Pg 10, line 6: I think the comparison between the ballast scheme here and Weber et al., (2016) is unwarranted as this is not the focus of the manuscript. The Weber analysis derives from an inversion of nutrient distributions and so represents the net effect of any number of potential processes. Any differences might therefore reflect the importance of other processes other than ballasting in some regions.

We removed the direct comparison of our results to those of Weber et al., and focus on the comparison with direct flux data in the revised manuscript.

Pg 11, line 7: I am unfamiliar with this approach to modelling atmospheric CO_2, where does 2.1 Gt C / 1 ppm relationship derive from?

The relationship is an estimate based on the mass of the atmosphere, the molar masses of CO_2, C and air, and the assumption that the air and CO_2 in the atmosphere are ideal gases.

One ppmv of atmospheric CO_2 is equivalent to a volume of CO_2 = (volume of the atmosphere * 10^{-6}). Since the volume of a gas is given by its mass m times its molar volume divided by its molar mass M, and assuming that the molar volumes of CO_2 and air are the same (assuming that they are ideal gases), the mass m of CO_2 equivalent to 1ppmv is given by $m_{CO2\_1ppm} = 10^{-6} * M_{CO2} * m_{atm} / M_{air}$, where M_{air} is the molar mass of dry air (28.96g/mol for 78.084% nitrogen, 20.946% oxygen, 0.934% argon and 0.03% CO_2), m_{atm} is the mass of the atmosphere (5.15×10^{18}kg, e.g., Trenberth and Smith, 2005), and M_{CO2} is the molar mass of CO_2 (44g/mol), which yields $m_{CO2_1ppm}\approx7.82$Gt. 7.82Gt of CO_2 are equivalent to $7.82Gt*M_{CO2}/M_C\approx7.82*44/12Gt\approx2.13Gt$ of carbon.

Figure 4: The CO_2 drawdown for the iron fertilisation (8 ppm) is lower than the published range mentioned in the Introduction (15 - 40 ppm). This needs some discussion, see also general comments.

In the revised manuscript, we further highlight that the simulated iron fertilization effect is solely due to the fertilization of cyanobacteria growth and therefore not comparable to the previous estimates from the literature. We further clarify that the focus of the manuscript is the description of the ballasting parameterization, and the estimate of the LGM dust ballasting effect on atmospheric CO_2. To this end, we removed "and iron addition" from the manuscript title, modified the abstract (now explicitly mentioning diazotroph and non-diazotroph effects in the last sentence), and we explain already in the introduction that the iron effect is likely underestimated (and why we still do look at the iron effect; page 3 lines 8-

12). We point out that this underestimation likely explains the deviation from previous estimates (page 17, lines 26-27).

Pg 14, lines 1-3: Does the weakening of the calcite export reflect a shift towards silicifying organisms? If so, does this also have an effect on ballasting sinking rates? i.e., is there a dual effect of ballasting from dust and from opal? I think these effects are quite interesting!

We do see a shift towards silicifying organisms in the simulation with LGM dust for iron fertilization (LGM_IRON), as reflected by reduced calcite export (see Fig. 2b in this document / response to the first reviewer) while opal export is enhanced (Fig. 9a, below). However, the global mean sinking speed in LGM_IRON hardly differs from that in the reference run with modern dust (PI_BALLAST; Fig. 9b), suggesting that the ballasting effect of the additional opal is balanced by the effect of the reduced calcite concentration.

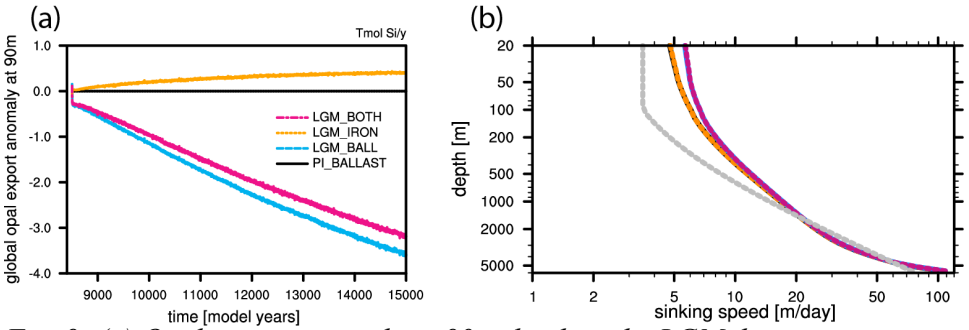

Fig. 9: (a) Opal export anomaly at 90m depth in the LGM dust sensitivity experiments using the dust only for ballasting (blue; LGM_BALL), only for iron fertilization (orange; LGM_IRON), and for both (pink; LGM_BOTH) relative to the pre-industrial reference with ballasting and modern dust (black, PI_BALLAST), and (b) global mean sinking speed profiles for the preindustrial reference run with particle ballasting (PI_BALLAST, black), and for the LGM sensitivity runs (colors as in panel a). For comparison, the gray dashed line in (b) is the applied Martin-type sinking speed in the PI reference run without ballasting.

This discussion was added to the revised manuscript (page 16, lines 9-13), and the panels a and b of Figure 9 (from this response / above) were added to the revised Fig. 5.

References

Heinze, C., Maier-Reimer, E., Winguth, A. M. E., & Archer, D. (1999). A global oceanic sediment model for long-term climate studies. Global Biogeochemical Cycles, 13(1), 221–250. http://doi.org/10.1029/98GB02812

van der Jagt et al. (2018). The ballasting effect of Saharan dust deposition on aggregate dynamics and carbon export: Aggregation, settling, and scavenging potential of marine snow. Limnology and Oceanography, 63(3), 1386–1394. http://doi.org/10.1002/lno.10779

Trenberth, K. E., & Smith, L. (2005). The Mass of the Atmosphere: A Constraint on Global Analyses. *Journal of Climate*, *18*(6), 864–875. http://doi.org/10.1175/JCLI-3299.1

Komar, P. D., Morse, A. P., Small, L. F., & Fowler, S. W. (1981). An analysis of sinking rates of natural copepod and euphausiid fecal pellets. Limnology and Oceanography, 26(1), 172–180. http://doi.org/10.4319/lo.1981.26.1.0172

Kriest, I., & Evans, G. T. (2000). A vertically resolved model for phytoplankton aggregation. Journal of Earth System Science, 109(4), 453–469. http://doi.org/10.1007/BF02708333

Lam, P. J., & Marchal, O. (2015). Insights into Particle Cycling from Thorium and Particle Data. Annual Review of Marine Science, 7(1), 159–184. http://doi.org/10.1146/annurev-marine-010814-015623

Response to Anonymous Referee #3

Heinemann et al. introduce a parameterization of the ballasting effect in the MPIOM/HAMOCC ocean model. This effect contributes to accelerate the export of POC (by reducing remineralization rates) and has the potential to strengthen the marine biological carbon pump, with consequence for atmospheric CO2 concentrations. Furthermore, the study investigates the consequences of enhanced Fe supply to the ocean on global export production during the last ice age (Martin hypothesis). The sensitivity experiments suggest that both effects only entail a rather limited (i.e. 12 ppmv) effect on atmospheric CO2, certainly leaning towards the lower end of available estimates from the literature.

This contribution is certainly both stimulating and timely and will certainly be of interest to the climate science community. I have to say, however, that the conclusions are somewhat weakened by the reduced sensitivity of the model to increased Fe availability. As mentioned below (last point), I would urge the authors to reconsider the modern Fe budget, which would allow the argumentation to be more relevant and certainly more convincing.

I'm not a climate modeler and as such have mostly concentrated on commenting the paleoclimatic/biogeochemical aspects of the manuscript. My comments are listed below.

As far as I understand the model set up does not account for the T-dependency of the remineralization length scale.

General comment

As shown by Kwon et al., 2009 (NGeo), the most important parameter accounting for enhanced sequestration of CO2 into the ocean interior results from the redistribution of remineralized carbon from intermediate to bottom waters. In essence, the depth at which POC is being remineralized is not critical as long as POC respiration takes place at intermediate depths, from which nutrients and CO2 can rapidly be resupplied to the fertile surface ocean, with negligible consequences for atmospheric CO2 concentrations.

However, if the bulk of POC remineralization takes place in the deep ocean cell, then CO2 can be sequestered away from the atmosphere for centuries to millennia. So in essence, if the ballasting effect does not allow POC to be exported to the deep ocean, then one would expect the consequences for atmospheric pCO2 to be small.

I was wondering if you could come up with some sense on how generally colder temperatures characteristic of the LGM in combination with the ballasting effect would affect atmospheric CO2 concentrations. I understand that adding T-dependent POC remineralization rates would be computationally expensive. But this aspect should at least be discussed in some more details.

As shown in Segschneider and Bendtsen (2013) for a HAMOCC global warming experiment, the inclusion of T-dependent remineralization has a more complex impact on the carbon sequestration than one would expect from a simple remineralization depth scale change (reduction for warming, increase for cooling). Compensating effects due to changes in remineralization and hence euphotic layer nutrient supply – driving changes in primary production – and further complication due to shifts in the ecosystem (opal vs. calcite producers) and resulting changes in surface alkalinity and hence CO_2-fluxes make it non-trivial to make any statements on the potential magnitude of including T-dependent remineralization on atmospheric CO_2. Segschneider and Bendtsen were planning to perform

corresponding experiments for a glacial ocean setup, but due to some unforeseen developments this has not materialized.

Maybe you could also consider adding a few sentences regarding the role of dissolved O2 concentration on remineralization rates, since intermediate waters were probably better ventilated/oxygenated during the LGM (e.g. Jaccard and Galbraith, 2012 (NGeo); Galbraith and Jaccard, 2015 (QSR)).

In the revised manuscript, effects of dissolved O2 concentrations on the simulated modern spatial transfer efficiency pattern are discussed (page 11, lines 21-26). We also highlight that ballasting effects can potentially modify the effects of changed oxygen concentrations during glacial cycles (page 18, lines 11-18).

Detailed comment

p. 1, l. 13 – Köhler et al., 2017 do not present any ice-core CO2 data. Please remove.

The 80ppm pCO_2 difference between the early Holocene and the LGM was estimated from the CO_2 data spline presented in Fig. 1a of Köhler et al. (2017). For that time period, the spline is based on data from the WAIS Divide Ice Core; we added the reference pointing directly to this data in the revised manuscript (Marcott et al. 2014).

p. 2, l. 3 - . . . "enhanced aridity", is probably more adequate that "enhanced desert"

We clarified: "… enhanced desert dust production and enhanced glacigenic dust production."

p. 2, l. 3-4 - please add appropriate references

We clarified that these are also results of the modelling studies referred to in the previous sentence (in particular, Mahowald et al., 2006).

p. 2, l. 16 – please consider citing Hain et al., 2010 (GBC)

Thanks, the reference was added to the list.

p. 11, l. 24-25 – please note that this observation is consistent with paleoceanographic observations, which suggest enhanced export production in the South Atlantic during the LGM as a result of Fe-bearing dust fertilization (e.g. Kumar et al., 1995 (Nature), Martinez-Garcia et al., 2014 (Nature), Anderson et al., 2014 (Phil. Trans. R. Soc.)). Furthermore, using stable nitrogen isotopes as a proxy for the relative nitrate consumption by phytoplankton, Martinez-Garcia et al., 2014 (Nature) showed that the biological carbon pump was not only stronger but also more efficient, in line with the argument outlined here.

Thank you for pointing the references out to us. We added the references to the introduction but decided that a comparison of the nitrate utilization changes reconstructed by Martinez-Garcia et al. to our results would bring us too far off track, also since the study is focused on iron fertilization effects and not on ballasting.

p. 14, l. 8-10 - As mentioned above, there is ample evidence suggesting enhanced export production in the Subarctic Zone of the Southern Ocean as a result of Fe- fertilization (see reference above), including outside of the direct influence of the Patagonian dust plume (e.g. Lamy et al., 2014 (Science). I am somewhat surprised that the model is not able to reproduce the paleoceanographic evidence.

Yes, we were also surprised and somewhat disappointed by that result (see response to your next comment). The disappointment turned into our motivation to fix this issue by using a more recent dust deposition field, but the implementation is still ongoing work.

p. 15 – I'm a bit puzzled by the final remarks. In essence you imply that Fe concentrations are too high in your control run, in part to the shortcomings associated with the study published by Mahowald et al., 2006. As a consequence, adding Fe to simulate glacial conditions will not entail much of an effect on atmospheric CO2 concentrations. This certainly weakens the conclusions of the sensitivity study. Wouldn't it thus be possible to include model runs including the downscaled modern dust input?

Understanding this may require a bit of a historical background: When starting our model development, we were not really aiming at an investigation of the iron fertilization effect on glacial pCO_2. Due to the standard model setup, however, in which dust is a source of iron, any change in the dust input intended to estimate the ballast effect on dust driven glacial pCO_2 decrease, will likewise have an effect on the amount of iron from the same dust input field. Therefore, we had to single out the effects of glacial dust on iron fertilization and enhanced settling velocities. And only then it turned out that the biological production was nowhere iron limited in the standard HAMOCC version. Likewise, we (both the authors of this study, and the model developers at MPI) were limited to the Mahowald et al. 2006 dust fields, as they were the only ones available with LGM/modern (and future) fields.

As discussed in our general response to all reviewers, we are currently working on the implementation of a more recent dust deposition reconstruction by Albani et al. (2016), which is expected to lead to iron limitation of phytoplankton growth rates in the simulated Southern Ocean, in line with modern observations. However, this development will take several months at least. And, because the lack of iron limitation occurs in both control simulations with and without ballasting and not only within the sensitivity runs, including the new dust field or using a dust field that is scaled down would require the repetition of the control simulations and of the sensitivity runs, and the release of a new standard version of HAMOCC, which we think is beyond the scope of this paper.

In the revised manuscript, we further highlight that the simulated iron fertilization effect is solely due to the fertilization of cyanobacteria growth and not comparable to the previous estimates from the literature, and we clarify that the focus of the manuscript is the description of the ballasting parameterization and the estimate of the LGM dust ballasting effect on atmospheric CO_2. To this end, we removed "and iron addition" from the manuscript title, modified the abstract (now explicitly mentioning diazotroph and non-diazotroph effects in the last sentence), and we explain already in the introduction that the iron effect is likely underestimated (and why we still do look at the iron effect; page 3 lines 6-12).

References

Marcott, S. A., et al..: Centennial Scale Changes in the Global Carbon Cycle During the Last Deglaciation, Nature, 514, 616–619, https://doi.org/10.1038/nature13799, 2014.

Segschneider, J., and J. Bendtsen (2013), Temperature-dependent remineralization in a warming ocean increases surface pCO_2 through changes in marine ecosystem composition, Global Biogeochem. Cycles, 27, 1214–1225, doi:10.1002/2013GB004684.

Relevant changes not described in response to referees

Page 5, lines 24-25 in the revised manuscript previously read “We assume that, below the euphotic zone, all particulate matter forms aggregates…”.

In fact, we assume that ALL particulate matter forms aggregates, also within the euphotic zone. The text “below the euphotic zone”, which is a leftover from an earlier version of the manuscript (prior to submission to GMDD) when we had limited particle ballasting to below the euphotic zone (which we don’t do in any of the presented simulations), was hence deleted.

CO_2 drawdown due to particle ballasting ~~and iron addition~~ by glacial aeolian dust: an estimate based on the ocean carbon cycle model MPIOM/HAMOCC version 1.6.2p3

Malte Heinemann[1], Joachim Segschneider[1], and Birgit Schneider[1]

[1]Kiel University, Institute of Geosciences, Ludewig-Meyn-Strasse 10, 24118 Kiel, Germany

Correspondence to: Malte Heinemann (malte.heinemann@ifg.uni-kiel.de)

Version: Tuesday 12th March, 2019, 01:14h

Abstract. Despite intense efforts, the mechanisms that drive glacial–interglacial changes in atmospheric pCO_2 are not fully understood. Here, we aim at quantifying the potential contribution of aeolian dust deposition changes to the atmospheric pCO_2 drawdown during the Last Glacial Maximum (LGM). To this end, we use the ocean circulation and carbon cycle model MPI-OM/HAMOCC, including a new parameterisation of particle ballasting that accounts for the acceleration of sinking organic soft tissue in the ocean by higher density biogenic calcite and opal particles, as well as mineral dust. Sensitivity experiments with reconstructed LGM dust deposition rates indicate that the acceleration of detritus by mineral dust ~~likely~~ played a small role for atmospheric pCO_2 variations during glacial–interglacial cycles – on the order of 5 ppmv, compared to the reconstructed ~80 ppmv-rise of atmospheric pCO_2 during the last deglaciation. The additional effect of the LGM dust deposition, namely the enhanced fertilisation by the iron that is associated with the glacial dust, likely played a more important role – ~~leading to a pCO_2-drawdown by more than 8 ppmv in our LGM sensitivity experiments despite an underestimated~~ although the full iron fertilization effect can not be estimated in the particular model version used here due to underestimated present-day non-diazotroph iron-limitation~~in the used model setup~~, fertilization of diazotrophs in the tropical Pacific already leads to an atmospheric pCO_2 drawdown of around 10 ppmv.

1 Introduction

According to ice core data ~~(Lüthi et al., 2008; Köhler et al., 2017)~~(Lüthi et al., 2008; Marcott et al., 2014; Köhler et al., 2017) , the atmospheric CO_2 concentration during the Last Glacial Maximum (LGM, ~21 thousand years ago) was about 80 ppmv lower than during the early Holocene. Model simulations show that the reduced atmospheric CO_2 concentration caused a global cooling, and, combined with orbital effects on Earth's climate, allowed the Laurentide, Cordilleran, British and Scandinavian ice sheets to build up (Abe-Ouchi et al., 2007; Heinemann et al., 2014; Ganopolski and Brovkin, 2017). It is still a matter of active discussion, however, which of the many potential climate and carbon cycle changes in response to the orbital forcing caused how much of the atmospheric pCO_2 drawdown (e.g., Brovkin et al., 2012; Chikamoto et al., 2012; Ganopolski and Brovkin, 2017).

Here we introduce a new parameterisation of the effect of higher density particles such as calcite, opal and dust on the sinking speed of detritus into the ocean circulation and carbon cycle model MPIOM/HAMOCC. Based on this new model setup, we estimate to what extent enhanced aeolian dust deposition contributed to the reconstructed atmospheric pCO_2 drawdown during the last glacial period due to ~~1)~~ its effect on particle ballasting~~, and 2) the enhanced iron fertilization associated with the dust~~.

Observationally constrained simulations of the global dust cycle have suggested that dust production and deposition rates were at least twice as large during the LGM compared to the Holocene and present~~(e.g., Werner et al., 2002; Mahowald et al., 2006; Albani . The increased aeolian dust emissions were due to both, enhanced desert and~~ , due to 1) enhanced desert dust production, and 2) enhanced glacigenic dust production (e.g., Werner et al., 2002; Mahowald et al., 2006; Albani et al., 2016). The increased desert dust production was caused mainly by a reduction in terrestrial vegetation (leading to larger desert dust source areas) due to inverse CO_2-fertilisation, temperature, precipitation and cloudiness changes (Mahowald et al., 2006) or by stronger tropospheric winds (Werner et al., 2002). Glacigenic dust, which is produced by the grinding of ice sheets and glaciers over the bedrock and sediments, and the subsequent transport of the produced fine sediment by meltwater beyond the ice margin (e.g., Bullard, 2013), contributed to the enhanced dust deposition, and globally, the magnitude of this glacigenic dust contribution was comparable to that of desert dust (Mahowald et al., 2006).

It is well known that enhanced glacigenic and desert dust deposition over the oceans can strengthen the biological carbon pump due to fertilisation with the bio-available iron contained in the dust (Martin, 1990; Kumar et al., 1995; Sigman and Boyle, 2000; Werner et al., 2002). This iron hypothesis is supported for example by mesoscale iron enrichment experiments which demonstrated that primary production in one third of the world ocean is limited by iron-availability (Boyd et al., 2007). Various modelling studies testing the iron hypothesis have concluded that a range of 15-40 ppmv of the reconstructed 80 ppmv atmospheric pCO_2 difference can be explained by iron fertilisation due to dust deposition changes ~~(Watson et al., 2000; Bopp et al., 2003; Brovkin et al., 2007; Lambert et al., 2015; Ganopolski and Brovkin, 2017)~~(Watson et al., 2000; Bo
.

Enhanced dust deposition can also have an effect on the sinking speed and remineralisation length scale of particulate organic carbon (POC or detritus). Detritus sinks because of its higher density compared to seawater (excess density). As aggregates including POC form, ballast minerals, i.e., silicate and calcite biominerals, as well as lithogenic minerals such as aeolian dust, which are more dense than organic tissue and seawater, provide a major weight fraction of sinking particles in the deep ocean (Honjo et al., 1982). Hence, ballast minerals contribute largely to the excess density of aggregates including detritus in the deep ocean. This led to the hypothesis that ballast minerals determine accelerated deep-water POC fluxes (ballasting hypothesis; e.g., Armstrong et al., 2002). Several deep-moored sediment trap observations of particle flux rates supported this ballasting hypothesis (see Boyd and Trull, 2007, for a review). While, e.g., Klaas and Archer (2002) and François et al. (2002) confirmed the association of calcite minerals with efficient transfer of POC to the deep ocean but suggested that the role of lithogenic minerals is negligible (see also Berelson, 2001), ~~a more recent study indicated~~ Dunne et al. (2007) suggested that neglecting lithogenic material in carbon cycle models would lead to an underestimation of the POC flux to the seafloor by 16-51 % globally~~(Dunne et al., 2007)~~. Noticeably high sinking speeds off Northwest Africa ~~are also in line with~~ (Fischer and Karakaş, 2009), and artificial dust deposition experiments using natural plankton communities from

off Mauritania and Saharan dust (van der Jagt et al., 2018) further support the hypothesis that ~~the deposition of Saharan dust accelerates~~ dust deposition can accelerate the sinking of detritus~~(Fischer and Karakaş, 2009).~~ .

Still, to the best of our knowledge, the hypothesis that particle ballasting changes due to variations of fluxes of lithogenic material into the ocean contributed to the reconstructed atmospheric pCO_2 changes during glacial–interglacial cycles (Ittekkot, 1993) has not yet been tested using ocean–biogeochemical models.

This manuscript is organised as follows. In Section 2, we describe our configuration of the ocean circulation and carbon cycle model MPIOM/HAMOCC (Section 2.1), introduce a simple particle ballasting scheme that includes the effect of lithogenic minerals from aeolian sources (Section 2.2), and describe the spinup procedure of the model (Section 2.3). In Section 3, we describe the necessary adjustment of HAMOCC parameters to the modified sinking speeds (Section 3.1) and compare the resulting reference simulation with the new particle ballasting to a reference simulation with the standard prescribed particle sinking speeds, and to observations (Section 3.2). In Section 4, ~~to estimate the effect of dust deposition changes on glacial–interglacial atmospheric pCO_2 variations,~~ sensitivity experiments with respect to LGM instead of modern dust deposition rates are presented ~~. We~~ to estimate the role of particle ballasting changes for galcial–interglacial atmospheric pCO_2 changes. Since the dust deposition fields are also used to compute the concentrations of bioavailable iron in HAMOCC, the LGM dust deposition changes have two effects, enhanced particle ballasting and iron fertilization. We isolate these two effects from each other, but will also show that the iron fertilization effect in the particular model version used in this study underestimates the observed present-day iron limitation in the Southern Ocean, likely leading to an underestimation of the iron fertilization effect of enhanced LGM dust depostion. We conclude with a summary and discussion of our results (Section 5).

2 Methods

To quantify the effect of aeolian dust variations on atmospheric pCO_2, we use the Max-Planck-Institute Ocean Model MPIOM and the embedded Hamburg Ocean Carbon Cycle model HAMOCC (Section 2.1). To account for particle ballasting effects, the default prescribed Martin-type sinking for detritus and the constant sinking speeds for opal, dust and calcite are replaced by a simple prognostic particle ballasting parameterisation following Gehlen et al. (2006), which assumes that detritus and the heavier particles form aggregates that sink at speeds computed from the density differences between these imaginary aggregates and the surrounding seawater (Section 2.2). The particle ballasting parameterisation derived here following Gehlen et al. (2006) differs for example from another approach that assumes that only a fraction of POC is sinking in association with ballast (e.g., Klaas and Archer, 2002; Armstrong et al., 2002; Howard et al., 2006; Hofmann and Schellnhuber, 2009). Note that the particle ballasting parameterization is, implicitly, also the very simplest aggregation model possible – assuming that all particulate matter instantly forms homogeneous aggregates, neglecting the complex biological and physical aggregation and disaggregation processes that occur in reality (e.g., Lam and Marchal, 2015) or that are explicitly captured in more complex (and computationally more expensive) aggregation models (e.g., Kriest and Evans, 2000).

Using the new particle ballasting parameterisation, we then perform sensitivity tests to quantify the effect of dust deposition changes on the atmosphere–ocean CO_2 fluxes, separating the effects of 1) particle ballasting by the dust, and 2) fertilisation

by the bio-available iron associated with the dust. The presented sensitivity tests are ~~equilibrium~~ simulations with prescribed modern or LGM dust deposition fields, atmospheric climatological forcing representing modern conditions, and pre-industrial greenhouse gas concentrations (GHGs). The atmosphere–ocean CO_2 flux anomalies in the simulations with LGM dust are used to estimate the effect of dust changes on atmospheric pCO_2 variations during glacial cycles. We do not perform transient simulations of glacial cycles yet, because 1) dust deposition fields are currently only available for snapshots during the last deglaciation, and 2) the computational cost and required wall-time to transiently simulate a glacial cycle or inception is currently too large.

2.1 Configuration of MPIOM/HAMOCC

Our results are based on the ocean-only model configuration of the Max-Planck-Institute Earth System Model (MPI-ESM; Giorgetta et al., 2013) version 1.2.00p4, which contains MPIOM version 1.6.2p3 (corresponding to revision 3997). MPI-ESM is a comprehensive Earth system model that consists of the atmosphere general circulation model ECHAM (Stevens et al., 2013), the land surface scheme JSBACH (Raddatz et al., 2007), and the ocean circulation model MPIOM (Jungclaus et al., 2013), which contains the ocean biogeochemistry model HAMOCC (Ilyina et al., 2013; Paulsen et al., 2017) including a sediment module (Heinze et al., 1999). MPI-ESM has been used successfully for millennial-scale atmosphere–ocean–carbon cycle simulations, including a transient simulation of the last millennium with fully interactive atmospheric CO_2 (Jungclaus et al., 2010). Since our aim is to isolate the effect of particle ballasting changes in the ocean during glacial–interglacial cycles on the atmosphere–ocean CO_2 fluxes, rather than realistically simulating past climate evolution, we use the ocean–only configuration of MPI-ESM, namely MPIOM/HAMOCC in stand-alone mode (Marsland et al., 2003; Maier-Reimer et al., 2005; Paulsen et al., 2017). ~~However,~~

However, for the sensitivity experiments with LGM dust deposition fields, we do consider variable atmospheric pCO_2 with a simple atmospheric CO_2 box model based on atmosphere–ocean CO_2 flux anomalies ~~(Section ??). This way,~~ relative to a reference simulation with modern dust deposition and ballasting (PI_BALLAST). The flux anomalies are diagnosed at the end of each simulated year, and the prescribed atmospheric pCO_2 is updated accordingly. For an accumulated net atmosphere–ocean CO_2 flux anomaly of 2.1 Gt C into the ocean, the atmospheric CO_2 concentration is reduced by 1 ppmv. Note that only the surface ocean biogeochemistry responds to this atmospheric pCO_2 feedback. There is no effect on the atmospheric radiative transfer or climate; the prescribed climatological atmospheric forcing is unchanged. If the atmospheric CO_2 concentration was not adjusted to the flux anomalies, a for example positive anomalous ocean CO_2 uptake would not result in a reduced atmospheric pCO_2, the atmosphere would behave like a CO_2 reservoir in our experiments, and the subsequent ocean CO_2 uptake would be overestimated (as illustrated by an additional experiment in Section 4.1 with LGM dust deposition for particle ballasting but without adjusting atmospheric pCO_2, shown as a blue dashed line in Fig. 5b). The long-term net ocean CO_2 uptake in our reference simulations (Fig. 5b) would lead to a negative CO_2 trend, if absolute atmosphere–ocean CO_2 fluxes were used; we avoid this effect by computing atmospheric CO_2 from the flux anomalies relative to the reference simulation in each year. Moreover, this approach of computing flux anomalies each year, compared to, e.g., the alternative of subtracting the mean flux imbalance of the reference run, avoids additional atmospheric pCO_2 variability due to, e.g., internal variability

of the ocean circulation. By using this simple atmospheric pCO_2 box model in combination with MPIOM/HAMOCC rather than using the coupled MPI-ESM, atmosphere and land surface feedbacks to the pCO_2 variations – that would alter the ocean circulation and complicate the analysis of dust-related CO_2 flux anomalies – are avoided, and computational time is saved.

Another measure to save computational time is the use of ~~the~~ a relatively coarse pre-defined, ~~coarse,~~ bi-polar~~ocean model grid setup~~ , curvilinear ocean grid (GR30L40~~. The grid poles are located over Greenland and Antarctica; the curvilinear grid has~~) with a grid-point spacing of ~~approximately~~ ~3°, and 40 levels with thicknesses ranging from 10-12 m in the upper ocean to 600 m in the deepest ocean.

The ocean model MPIOM is forced by a repeating 1-year-long climatology of daily mean surface boundary conditions, including 2 m air temperature, zonal and meridional windstress, windspeed, shortwave radiation, total cloud cover, precipitation and river runoff, representing modern conditions based on the ERA40 and ERA15 reanalyses (Röske, 2005, 2006) as in Paulsen et al. (2017).

To avoid salinity trends due to imbalances of precipitation, evaporation, and river runoff, the surface salinity is restored with a relaxation coefficient of $3.3{\cdot}10^{-7}$ s^{-1} to the annual salinity field of the Polar science center Hydrographic Climatology (PHC).

Note that biogeochemical changes do not affect the ocean circulation in the default (and our) configuration of MPIOM/HAMOCC. That means, for example, any effect of phytoplankton concentration changes on light absorption (Wetzel et al., 2006) is neglected in MPIOM. Differences in the ocean circulation between our simulations with the standard MPIOM/HAMOCC setup and the setup that includes particle ballasting are only due to the fact that, unfortunately, different numbers of CPUs were used for the computations (Fig. 1a: black lines cover green and brown lines, but not the dark grey line of the setup without ballasting). For binary-identical results, the parameter 'nprocx' must not be changed. Otherwise, the spatial and temporal variations of the ocean circulation would be identical in the spinup with the standard model and the simulations with ballasting.

2.2 Particle sinking and ballasting in HAMOCC

In the standard version of HAMOCC, particle ballasting is not accounted for. Calcite and opal shells sink at a prescribed, constant speed of 30 m day^{-1}; dust sinks at a speed of only 0.05 m day^{-1}, resulting from the assumption of spherical dust particles with a diameter of 1 μm following Stokes' law (Stokes' drag is balanced by gravitational force minus buoyancy force); the sinking speed of detritus w_{det} is constant in the euphotic zone, and increases with depth z below the euphotic zone ($z > 100$ m) following Martin et al. (1987):

$$w_{det}(z) = w_{eu} + \begin{cases} 0, & z \leq 100 \text{ m} \\ \frac{\lambda_{det}}{b}(z - 100 \text{ m}), & z > 100 \text{ m}, \end{cases} \quad (1)$$

where $w_{eu} = 3.5$ m day^{-1} is the sinking speed in the euphotic zone, the parameter b is set to 2, and the remineralisation rate for detritus λ_{det} is set to 0.0025 day^{-1}, resulting in sinking speeds up to 80 m day^{-1} (Fig. 2b).

To account for particle ballasting, we add a simple parameterisation of particle sinking speeds to HAMOCC. We assume that ~~, below the euphotic zone,~~ all particulate matter forms aggregates and sinks together at a common speed $w_{ballast}$. As suggested

by Gehlen et al. (2006), the common speed is proportional to the difference between the mean density of all particles $\rho_{particles}$ and the density of the seawater ρ_{sw} in each model grid box:

$$w_{ballast} = w_0 \cdot \frac{\rho_{particles} - \rho_{sw}}{\rho_{det} - \rho_{sw}}. \quad (2)$$

w_0 is the proportionality factor, and can be interpreted as the sinking speed of the aggregate in the ~~absense~~ absence of particle ballast. The density difference $\rho_{particles} - \rho_{sw}$ is also called excess density. The mean density of all particles $\rho_{particles}$ is given by the mass of all particles per unit volume of seawater, divided by the volume of all particles per unit volume of seawater. In contrast to Gehlen et al. (2006), here, dust also contributes to the ballasting of detritus:

$$\rho_{particles} = \frac{c_{dust} + \sum_b m_b \Psi_b}{\frac{1}{\rho_{dust}} c_{dust} + \sum_b \frac{m_b}{\rho_b} \Psi_b}, \quad (3)$$

where c_{dust} is the mass concentration of dust ~~,~~ (mass of dust per unit volume of seawater, in g cm^{-3}), ρ_{dust} is the density of dust (2.50 g cm^{-3}), Ψ_b are the molar concentrations of the biogenic particle types b (namely: detritus, calcite, and opal, in mol C and mol Si per cm^3, respectively), m_b are their molar masses (32.7 g (mol C)$^{-1}$ for detritus, 100.0 g (mol C)$^{-1}$ for calcite, and 72.8 g (mol Si)$^{-1}$ for opal) and ρ_b are their densities (1.06 g cm^{-3} for detritus, 2.71 g cm^{-3} for calcite, and 2.10 g cm^{-3} for opal).

Monthly mean dust deposition rates are prescribed based on numerical reconstructions for modern and LGM boundary conditions, including glacigenic dust (Fig. 6a-b; Mahowald et al., 2006). The dust deposition fields not only affect the sinking speed in our ballasting parameterisation, but also the availability of iron. It is assumed that 3.5 % (weight) of the dust in the water column is iron, of which 1 % is soluble and bio-available.

2.3 Spinup of the standard model setup

Before starting our experiments with particle ballasting, we spin-up the standard version of MPIOM/HAMOCC without particle ballasting for over 10,000 years (Fig. 1). During the spin-up phase, the ocean model, which is initialised from three-dimensional PHC temperature and salinity fields, approaches an equilibrium state (thanks to the salinity-restoring at the surface). The simulated ocean circulation is characterised by deepwater formation in the Atlantic and Southern Ocean, and no deepwater formation in the Pacific; the Atlantic meridional overturning at 26° N amounts to about 17 Sv (Sverdrup; 10^6 m^3 s^{-1}; Fig. 1a).

The ocean carbon cycle is not so easily tamed, since it remains an open system in our model (no restoring). To reach a stable equilibrium of the carbon cycle in the water column and the sediment, the net fluxes of organic carbon, calcite and opal from the ocean column to the sediment – which are computed in HAMOCC – need to be balanced by the fluxes into the ocean of organic matter, calcite and silicate from weathering on land – which are prescribed as namelist parameters (called deltaorg, deltacal, and deltasil). The weathering fluxes are adjusted several times during the spinup phase, aiming at 1) balancing the sediment burial fluxes as diagnosed from the trends in the sediment inventory over several hundred years prior to each weathering flux adjustment, 2) a stable calcite export production at 90 m depth of about 1 Gt C yr^{-1}, and 3) a rain ratio (ratio of calcite export to detritus export at 90 m depth) of about 10 % (Fig. 1f). An equilibrium of the sediment, however, is not reached in our simulations. Note that the selection of the weathering fluxes itself affects the simulated biogeochemistry. For example, if the

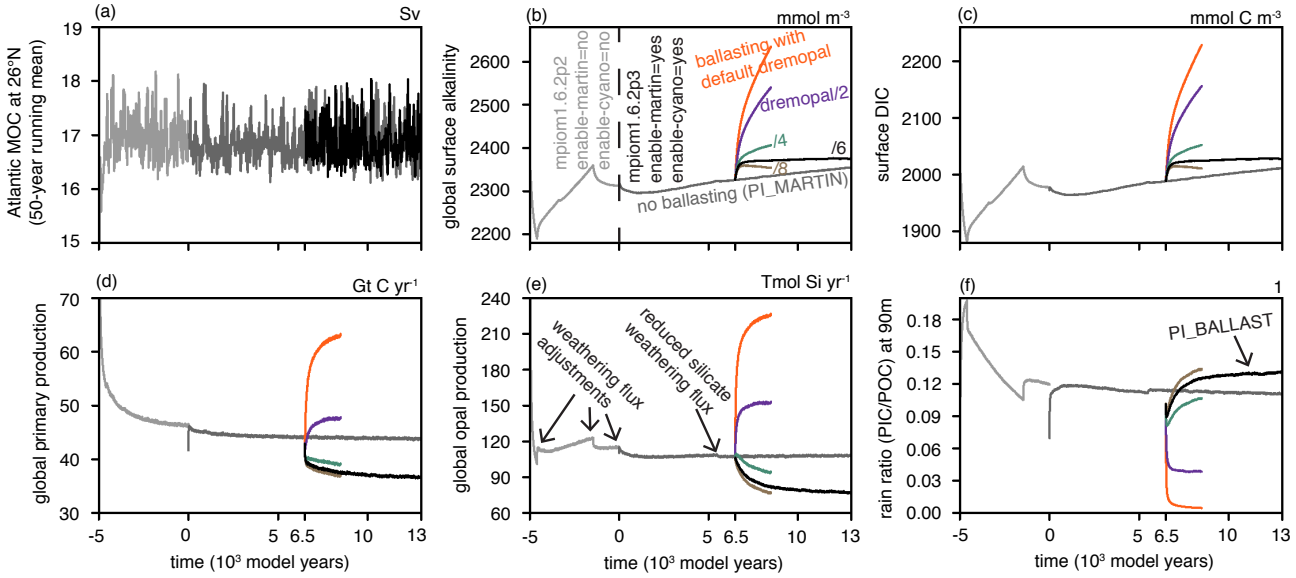

Figure 1. Selection of the weathering rates during the spinup of MPIOM/HAMOCC, and adjustment of the opal remineralisation rate to modified sinking speeds. a, Strength of the Atlantic Meridional Overturning Circulation (AMOC) at 26° N; b, surface alkalinity; c, surface dissolved inorganic carbon (DIC); d, global primary production; e, global opal production; and f, ratio of global calcite to organic carbon export at 90 m depth (rain ratio). The initial 5000-year long simulation was done with an older MPIOM/HAMOCC setup; we do not intend to interpret the biogeochemistry of this run. However, the endpoint of this older simulation is used as a starting point for our modern control simulation without particle ballasting, using the default-configuration of MPIOM/HAMOCC in MPI-ESM 1.2.00p4, including a new parameterisation of diazotrophs (Paulsen et al., 2017) and Martin-type sinking (darker grey). In model year 6500, the ballasting parameterisation is switched on, and, to compensate for the reduced sinking speed of opal in the euphotic zone, the opal dissolution rate λ_{opal} (namelist parameter dremopal) is reduced from 0.01 day^{-1} by factors of 2, 4, 6 and 8.

silicate weathering flux is increased, more opal can be produced, and calcite production is suppressed (see Eqs. 12-14 of Ilyina et al., 2013).

3 Results for modern dust deposition

To simulate a reasonably realistic carbon cycle with atmosphere–ocean CO_2 fluxes comparable to observations, and to create a mean state with particle ballasting that is very close to the mean state of the standard setup, it is important to adjust HAMOCC to the substantially modified particle sinking speeds that result from the particle ballasting parameterisation. In this section, we argue that this adjustment can be achieved by a reduction of the opal dissolution rate (Section 3.1) and then compare the resulting carbon cycle simulation with particle ballasting ~~to a~~ (PI_BALLAST) to the simulation with the standard prescribed / Martin-type POC sinking (PI_MARTIN), and to observational data (Section 3.2).

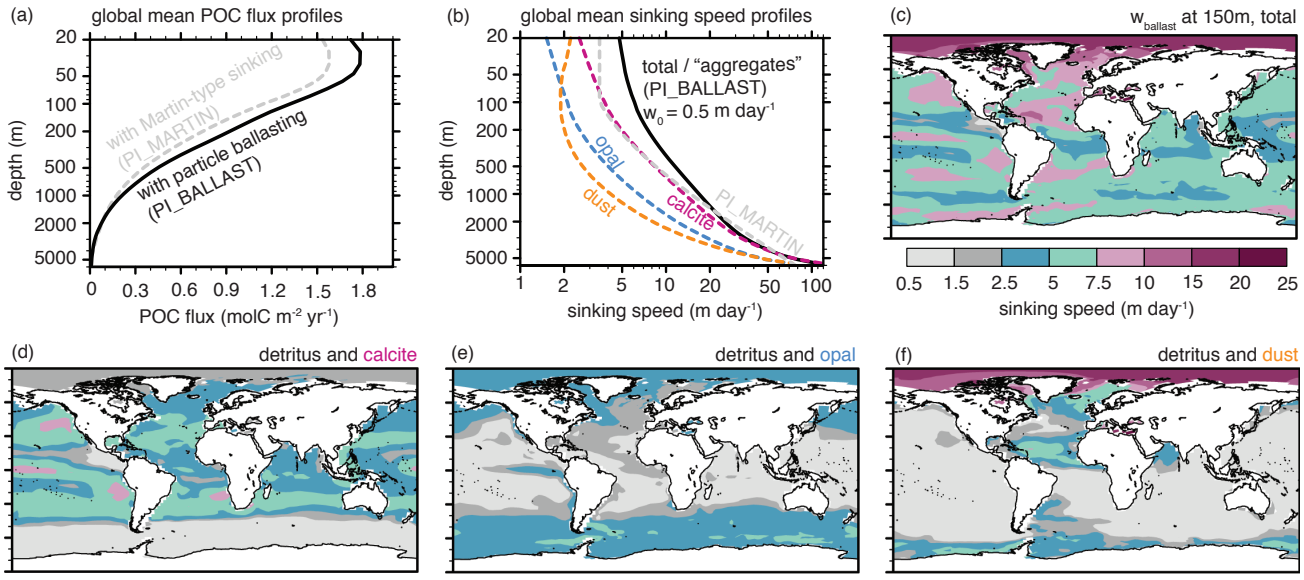

Figure 2. ~~Particle~~ Global mean particulate organic carbon (POC) flux profiles (a) and particle sinking speed $w_{ballast}$ for ~~a~~b, global mean profiles and ~~b-e~~c-f, at 150 m depth. The contributions of the different ballast types (calcite, opal, and dust) to the resulting, applied "aggregate" sinking speed (black) are estimated by re-computing the sinking speed assuming that only one type of ballast is present. The dashed grey line in panel a shows the Martin-type sinking speed applied to POC in every watercolumn in the reference simulation without ballasting (PI_MARTIN). Note the logarithmic depth scale~~, the euphotic zone is indicated by grey shading~~.

3.1 Adjusting HAMOCC to the new particle sinking

The simulations with particle ballasting are initialized from year 6500 of the reference simulation without particle ballasting (PI_MARTIN; Fig. 1b). Using a no-ballast reference speed w_0 (Eq. 2) of 0.5 m day^{-1} leads to global mean sinking speeds $w_{ballast}$ of the virtual aggregates between about 5 m day^{-1} at the surface and about 120 m day^{-1} below 5 km depth (Fig. 2~~a~~b). A larger w_0, such as 3.5 m day^{-1} as used by Gehlen et al. (2006), would lead to much higher global mean sinking speeds. The advantage of using the small w_0 is that it yields global mean aggregate sinking speeds that are comparable to the depth-dependent, Martin-type sinking speed of detritus that is prescribed in ~~the standard control simulation~~ PI_MARTIN (Fig. 2~~a~~b), and to a similar POC flux profile (Fig. 2a), which allows us to avoid a re-tuning of the remineralisation rate of detritus.

The dissolution rate of opal, however, needs to be re-tuned, since the sinking speed of opal is reduced from previously 30 m day^{-1} to now only ~5 m day^{-1} in the euphotic zone (Fig. 2~~a~~b). Consequently, more opal is dissolved within the euphotic zone, leading to higher silicate concentrations, a higher opal production rate (Fig. 1e), and a very low rain ratio (Fig. 1f) due to a completely suppressed calcite production. Without adjusting the river input (weathering) of calcite to the reduced calcite precipitation and burial, surface alkalinity and DIC rise (Fig. 1b-c). For a reduction of the opal dissolution rate by a factor of 6, the trends in alkalinity and DIC become small, and comparable to (or, actually smaller than) the trend in the control simulation

without ballasting (Fig. 1b-c), and, even without re-adjusting the weathering fluxes, a stable carbon cycle simulation with particle ballasting (PI_BALLAST) is achieved that is similar to ~~the control simulation without ballasting~~PI_MARTIN.

3.2 Ballasting effects and comparison to observations

For pre-industrial GHGs (pCO_2=278 ppmv), modern ocean circulation, and modern dust deposition (Fig. 6a), the simulated atmosphere–ocean CO_2 fluxes in the standard setup (PI_MARTIN) and the setup with particle ballasting (PI_BALLAST) are hardly distinguishable (Fig. 3b-c). There are, however, clear differences compared to the observed modern CO_2 fluxes (Fig. 3a). Most notably, the observed flux of CO_2 from the atmosphere into the ocean between 30° S and 60° S in the South Atlantic, Indian Ocean and West Pacific is underestimated, due to an overestimation of the ocean surface pCO_2, as previously reported for HAMOCC within the coupled MPI-ESM (Ilyina et al., 2013). Also note that the CO_2 flux data (Takahashi et al., 2009) is based on modern observations, while ~~in the model simulations,~~ pre-industrial GHGs are prescribed in the model simulations.

~~Similarly, the surface~~ A comparison of simulated to observed nutrient concentrations is shown in Fig. 3d-f for phosphate at the surface, and in a Taylor diagram (Fig. 4) at the surface, 100 m depth, and 2 km depth for phosphate, nitrate, and silicate. The surface dissolved phosphate concentrations are hardly distinguishable in the simulations with ~~and without ballasting~~particle ballasting (PI_BALLAST) and without particle ballasting (PI_MARTIN). Compared to observations (WOA, Garcia et al., 2013), the simulated phosphate concentrations in the Southern Ocean, Indian Ocean, Equatorial Pacific, and in the North Pacific are underestimated (Fig. 3d-f), and these biases are again similar to previous HAMOCC studies (Ilyina et al., 2013). This similarity between the simulated phosphate concentrations is not only true at the surface, but also at depth (Fig. 4). The large overestimation of the spatial variability of the phosphate concentrations at 2 km depth in both simulations is due to an underestimation of the concentrations in the Atlantic and an overestimation in the eastern tropical Pacific (not shown). For nitrate, the observed high concentrations in the Antarctic circumpolar region at the surface and 100 m depth are underestimated in both simulations, leading to an underestimated spatial variability at these depths (Fig. 4). At 2 km depth, the simulation with particle ballasting fits better to observations (Fig. 4), especially due to an improved fit in the eastern Pacific (nitrate concentrations are overestimated in the eastern Pacific in PI_MARTIN, while they fit relatively well in PI_BALLAST; not shown). For silicate concentrations, the fit to observations is improved at the surface and in 100 m depth in the simulation with particle ballasting, mostly because the concentrations in the Antarctic circumpolar region match observations well in PI_BALLAST, while they are overestimated in PI_MARTIN. At 2 km depth, the fit is also improved in PI_BALLAST due to a reduction of the positive concentration bias in the eastern Pacific (compared to PI_MARTIN).

The global primary production in the simulation with ballasting amounts to about 39 Gt C yr^{-1} compared to 44 Gt C yr^{-1} in the simulation without particle ballasting (Fig. 1d), not including the primary production by diazotrophs, which amounts to additional 5 Gt C yr^{-1} and 4 Gt C yr^{-1} for ~~the simulations with ballasting and the standard setup~~PI_BALLAST and PI_MARTIN, respectively. The global organic matter export is slightly reduced (7.0 Gt C yr^{-1} compared to 7.5 Gt C yr^{-1} without ballasting), and the global calcite production and export are only moderately larger (1 Gt C yr^{-1} compared to 0.85 Gt C yr^{-1} without ballasting, not shown), leading to an elevated rain ratio of about 13 % compared to 11 % in the simulation without ballasting (Fig. 1f). Opal production (Fig. 1e) and opal export at 90 m (not shown) are reduced by about 30 % in the simulation with

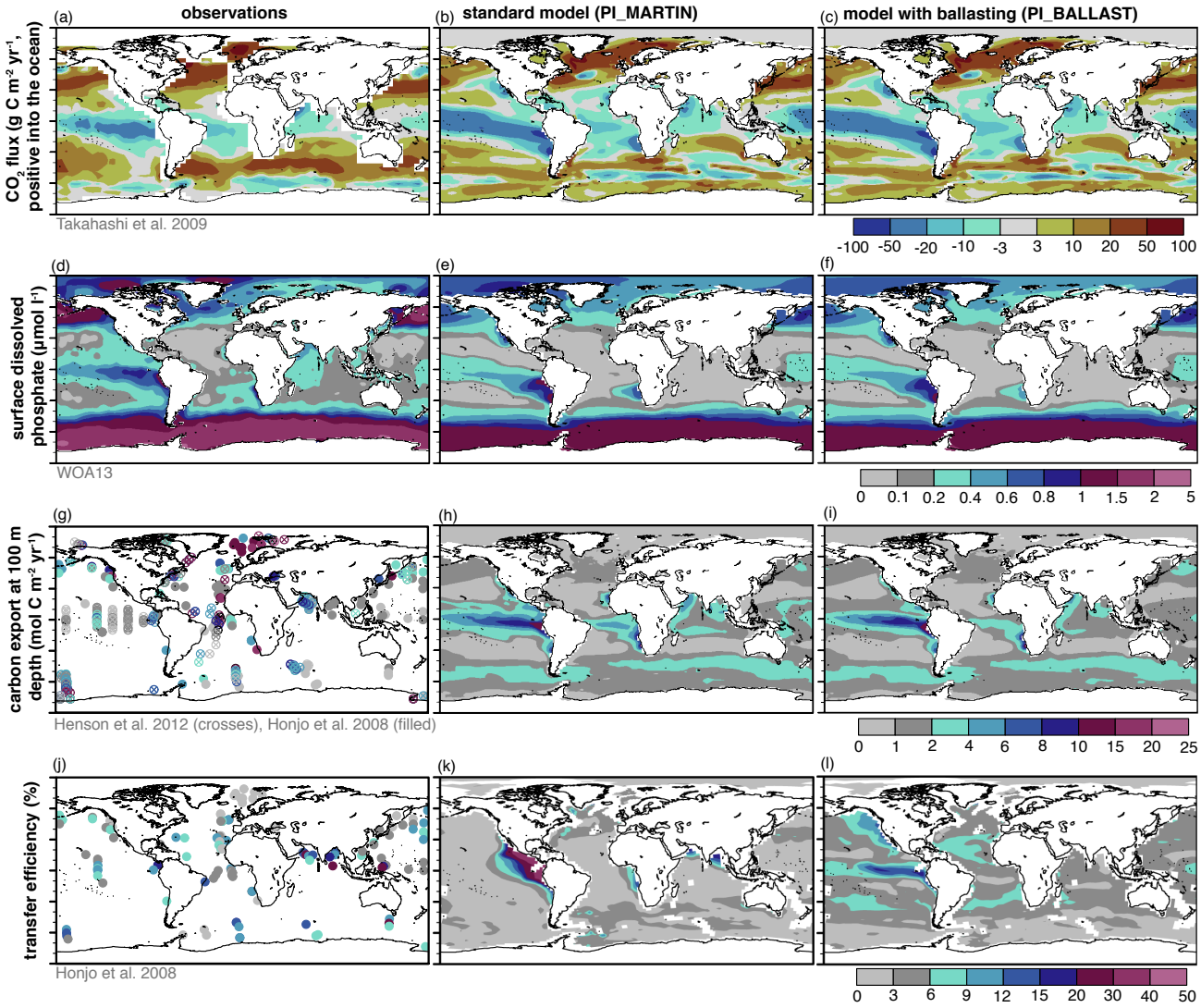

Figure 3. Comparison of the reference simulations with particle ballasting (PI_BALLAST) and without particle ballasting (standard setup with constant / Martin-type particle sinking; PI_MARTIN) to observations. a-c, net atmosphere-to-ocean CO_2 flux from observations (Takahashi et al., 2009) compared to our simulations; d-f, surface dissolved phosphate from the World Ocean Atlas (Garcia et al., 2013) compared to our ~~MPIOM/HAMOCC~~ simulations; g-i, carbon export at 100 m depth as derived from satellite data ~~(Henson et al., 2012, filled circles)~~ (Henson et al., 2012, crosses) and from sediment trap data ~~(Honjo et al., 2008, crosses)~~ (Honjo et al., 2008, filled circles) compared to the export at 90 m depth in our simulations; and j-l, transfer efficiency (carbon flux at ~~1000~~2000 m depth divided by the carbon flux at 100 m depth) as derived from sediment trap data (Honjo et al., 2008) compared to the 90 m to ~~960~~2080 m transfer efficiency in our simulations. For all simulations in this figure, modern dust deposition rates were prescribed; shown are averages computed over the model years 12900 to 12999.

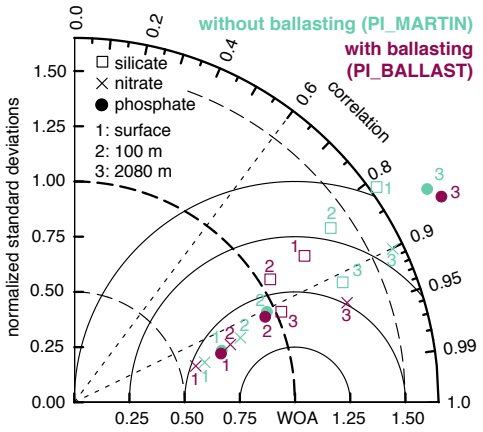

Figure 4. Taylor diagram comparing annual mean silicate (squares), nitrate (crosses), and phosphate concentrations (dots) at 3 different depths (numbers) of the preindustrial reference simulations with Martin-type sinking (PI_MARTIN, aquamarine) and with particle ballasting (PI_BALLAST, pink) to World Ocean Atlas data (WOA, Garcia et al., 2013).

modern dust and ballasting compared to the run without ballasting (production 76 versus 108 Tmol Si yr^{-1}, export 72 versus 103 Tmol Si yr^{-1}).

The simulated spatial pattern of the carbon export in ~~100~~90 m depth (export production) in ~~the standard model setup and the setup with ballasting~~ PI_MARTIN and PI_BALLAST are very similar to each other, with the area of high export production in the Equatorial Pacific extending further into the subtropics in ~~the standard setup~~ PI_MARTIN (Fig. 3h-i). Compared to estimates based on sediment trap data (Honjo et al., 2008) and satellite data (Henson et al., 2012), the simulated export production in both simulations is underestimated in the North Atlantic, and overestimated in the Equatorial Pacific (Fig. 3g-i).

Only a fraction of this export production from the euphotic zone reaches the deep ocean. This fraction, also called transfer efficiency, is a measure for the efficiency of the biological pump. ~~Compared to estimates based on sediment trap data (Honjo et al., 2008), the simulated transfer efficiency~~ The range of simulated transfer efficies through the mesopelagic zone (here computed as the simulated POC flux at ~~960~~2080 m depth divided by the POC flux at 90 m depth ~~) is too high for most of the sediment trap locations.~~

~~The mostly enhanced transfer efficiency in our simulation with ballasting compared to~~ in PI_BALLAST and PI_MARTIN) compares well with the range of transfer efficiency estimates based on sediment trap data (Honjo et al., 2008, Fig. 3j-l). In the simulation without ~~ballasting is in line with the higher global mean sinking speed between 100 m and 1000 m compared to the applied Martin-type sinking speed profile (~~particle ballasting (PI_MARTIN), the same sinking speed profile for POC is prescribed everywhere. Hence, the variations in the transfer efficiency are only due to local differences of the organic matter remineralization rate, which depends on oxygen availability. Denitrification and sulfate reduction remineralization rates combined are lower than aerobic remineralization rates (see Eq. 6 of Ilyina et al., 2013), leading to higher transfer efficiencies in oxygen minimum zones (OMZs), e.g., in the eastern Equatorial Pacific, Arabian Sea, and Bay of Bengal (Fig. 3k). In

the simulation with particle ballasting (PI_BALLAST), this effect of lower remineralization rates in OMZs is at least partly compensated by reduced ballasting by calcite due to the corrosive waters, resulting in lower settling speeds and transfer efficiencies (Fig. 3l). The relatively high transfer efficiencies in the mid-latitudes in PI_BALLAST compared to PI_MARTIN are in line with high particle sinking speeds mostly due to ballasting by calcite particles (compare Fig. 2~~a). d~~ to Fig. 3l).

However, as far as we understand, even qualitatively, the global pattern of transfer efficiencies is uncertain: On the one hand, Henson et al. (2012) suggested based on satellite data that, in large areas of the tropics and subtropics except in the eastern Equatorial Pacific cold tongue, over 30 % of the export production in 100 m depth reach the deep ocean below 2000 m, while at high latitudes (>50°) less than 10 % of the export production reaches that depth. On the other hand, Weber et al. (2016) ~~suggested~~ reconstructed from nutrient distributions a "global pattern of transfer efficiency to 1000 m that is high (∼25 %) at high latitudes and low (∼5 %) in subtropical gyres, with intermediate values in the tropics".

~~In our simulation with particle ballasting, the Equatorial Pacific cold tongue is characterised by high transfer efficiencies, and the subtropics by lower efficiencies, which better fits to the results of Weber et al. (2016) than to those of Henson et al. (2012) . However, our results do not support the high transfer efficiencies at high latitudes suggested by Weber et al. (2016), despite the fact that opal and dust particles lead to an acceleration of detritus in the Arctic and Southern Ocean in our simulations with particle ballasting (Fig. 2d-e). The relatively high transfer efficiencies in the mid-latitudes in our simulation with ballasting are in line with high particle sinking speeds mostly due to ballasting by calcite particles (compare Fig. 2c to Fig. 3l).~~

Dust substantially affects sinking speeds and the transfer efficiencies in the Southern Ocean and South Atlantic off Patagonia, as well as in the ~~Equatorial~~ equatorial Atlantic due to Saharan dust deposition, in the North Atlantic, and in the Arctic Ocean. Note, however, that, in particular in the Arctic Ocean, where POC concentrations are low, even small quantities of dust can lead to high sinking speeds, since our simple particle ballasting parameterisation only takes into account the density of the dust (in the limit of zero POC), and not its diameter. This leads to high sinking speeds in the model, while in reality, when POC concentrations are so low that particle collisions and aggregate formation are unlikely, the small and mostly individual dust particles sink very slowly according to Stoke's law. While this illustrates ~~the~~ a limitation of the simple particle ballasting parameterisation, the effect of the erroneously high sinking speeds in the Arctic on the carbon export is small: the integrated carbon export at 90 m depth north of 80° N amounts to only 0.01 Gt C yr^{-1}, or just over 0.1 % of the global export of about 7 Gt C yr^{-1}.

In summary, although the simulated sinking speeds substantially differ between the simulations with and without particle ballasting, the biases of the setup with particle ballasting compared to observations remain similar to the biases of the standard setup. But the setup with particle ballasting now enables us to estimate the effect of glacial dust deposition on atmospheric pCO_2.

4 Sensitivity to LGM dust deposition

4.1 ~~Experimental setup~~

Starting from the simulation with particle ballasting described in the previous section (PI_BALLAST, with the opal dissolution rate reduced by a factor of 6, modern dust deposition, modern ocean circulation and pre-industrial GHGs), 3 experiments are performed to estimate the sensitivity of the ocean carbon cycle to the reconstructed LGM dust deposition. In all 3 sensitivity experiments, the prescribed monthly-mean modern dust deposition fields are replaced instantaneously by monthly-mean LGM dust deposition fields (see Fig. 5 for timeseries of the sensitivity experiments, and Fig. 6a-c for maps of the annual mean dust deposition rates and the LGM-modern dust deposition difference). In the first experiment, the LGM dust deposition rates are only used for the computation of dust concentrations in the water column, isolating the ballasting effect of the LGM dust deposition (LGM_BALLAST; solid blue lines in Fig. 5). In the second experiment, the LGM dust deposition rates are only used for the computation of the bio-available iron concentrations, isolating the iron fertilisation effect associated with the dust (~~orange~~LGM_IRON; orange lines). In the third experiment, the LGM dust deposition is used for both, particle ballasting and iron fertilisation (~~pink~~LGM_BOTH; pink lines).

4.1 ~~Atmospheric pCO_2 feedback~~

~~To quantify the roles of particle ballasting and iron fertilisation by dust deposition changes for atmospheric pCO_2, the atmosphere–ocean CO_2 flux anomalies relative to the reference simulation with modern dust deposition (black lines in Fig. 5) are diagnosed at the end of each simulated year, and the prescribed atmospheric pCO_2 is updated accordingly. For an accumulated net atmosphere–ocean CO_2 flux anomaly of 2.1 Gt C into the ocean, the atmospheric CO_2 concentration is reduced by 1 ppmv. Note that only the surface ocean biogeochemistry responds to this atmospheric pCO_2 feedback. There is no effect on the atmospheric radiative transfer or climate; the prescribed climatological atmospheric forcing is unchanged.~~

~~If the atmospheric CO_2 concentration was not adjusted to the flux anomalies, a for example positive anomalous ocean CO_2 uptake would not result in a reduced atmospheric pCO_2, the atmosphere would behave like a CO_2 reservoir in our experiments, and the subsequent ocean CO_2 uptake would be overestimated. This is illustrated in a fourth experiment, in which LGM dust is prescribed for particle ballasting without applying the simple atmospheric pCO_2 box model described above (dashed blue line in Fig. 5a-b).~~

~~The long-term net ocean CO_2 uptake in our reference simulations (Fig.5b) would lead to a negative CO_2 trend in our simple CO_2 box model, if absolute atmosphere–ocean CO_2 fluxes were used; we avoid this effect by computing atmospheric CO_2 from the flux anomalies relative to the reference simulation in each year. Moreover, this approach, compared to, e.g., the alternative of subtracting the mean flux imbalance of the reference run, avoids additional atmospheric pCO_2 variability due to, e.g., internal variability of the ocean circulation.~~

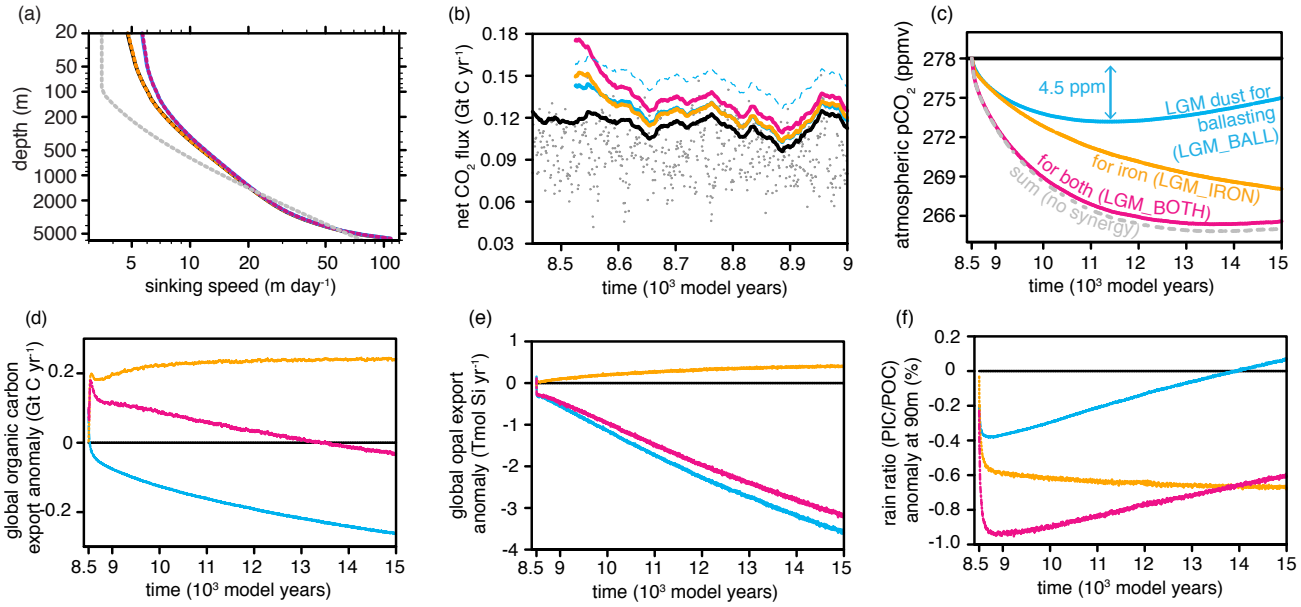

Figure 5. Effects of switching to LGM dust deposition for particle ballasting (LGM_BALL, blue), for the computation of iron fertilisation associated with the dust (LGM_IRON, orange), and for both (LGM_BOTH, pink) compared to the control simulation with ballasting and iron fertilisation based on modern dust deposition (PI_BALLAST, black). a, ~~estimated atmospheric pCO_2 change based on the annual~~ global mean ~~atmosphere–ocean CO_2 flux anomalies relative to~~ sinking speed profiles; gray dashed line indicates the ~~control run~~ Martin-type sinking speed profile as used in the standard simulation without ballasting (PI_MARTIN); note that the black curve (PI_BALLAST) is hidden behind the orange curve (LGM_IRON), and that the blue curve (LGM_BALL) is hidden behind the pink curve (LGM_BOTH); b, global mean atmosphere–ocean CO_2 fluxes; positive values indicate a net flux from the atmosphere into the ocean; solid lines are 50-year running means; the dots show annual means of the CO_2 fluxes in ~~the simulation with the standard setup without particle ballasting~~ PI_MARTIN to illustrate the large interannual variability (e.g., due to ocean circulation variability) compared to the dust-induced anomalies; the blue dashed line is the CO_2 flux in a simulation with LGM dust for ballasting where the atmospheric pCO_2 was *not* updated every year according to the atmosphere–ocean CO_2 flux anomalies of the previous year; c, atmospheric pCO_2 change based on the annual mean atmosphere–ocean CO_2 flux anomalies relative to PI_BALLAST; the gray dashed line shows the sum of the LGM_BALL and LGM_IRON pCO_2 change; d, global organic ~~matter~~ carbon export anomaly relative to PI_BALLAST in 90 m depth; ~~d~~e, global opal export anomaly relative to PI_BALLAST in 90 m depth; f, anomaly of the global ratio of particulate inorganic carbon (PIC, calcite) to particulate organic carbon (POC) within the particle export in 90 m depth.

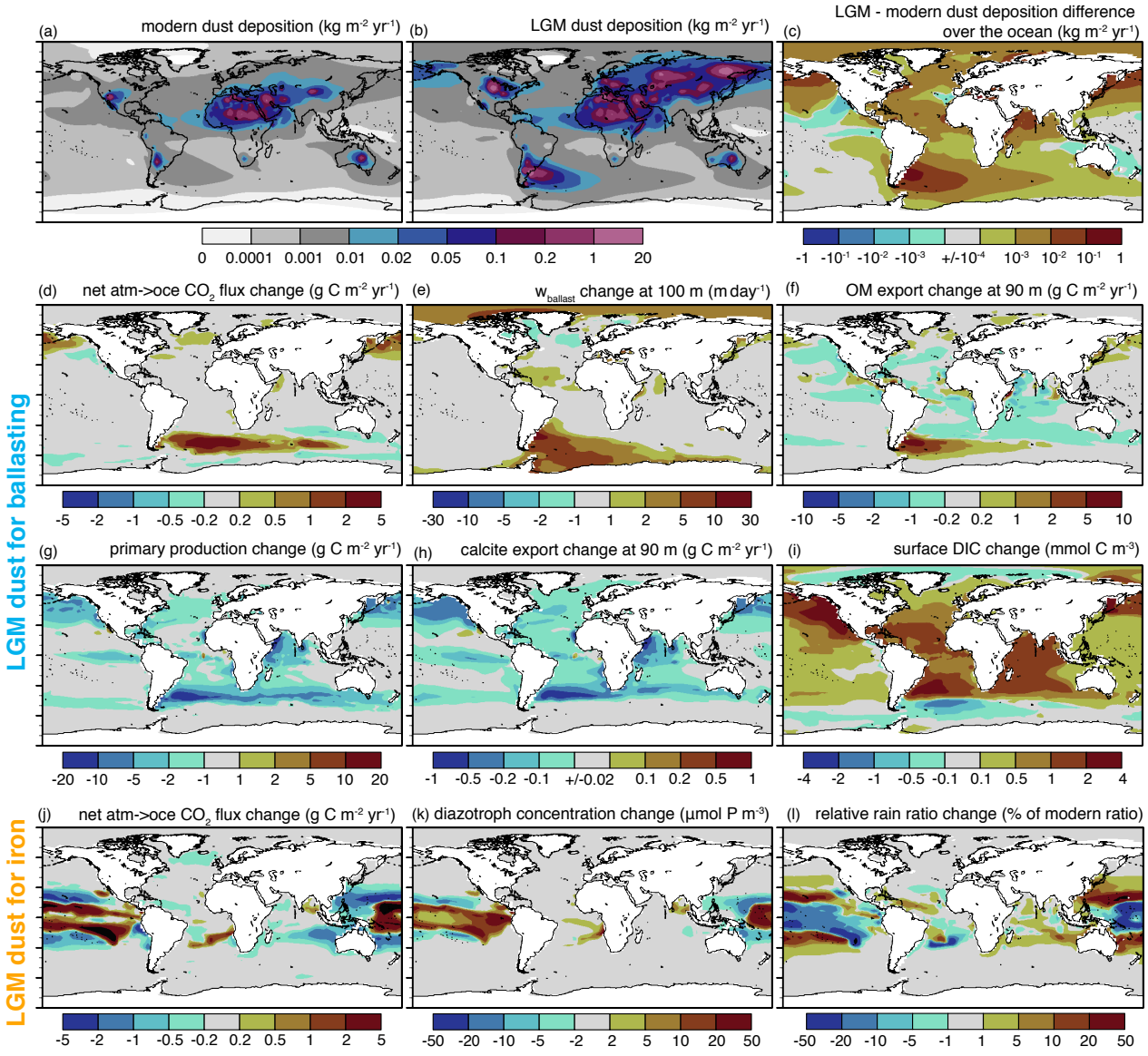

Figure 6. Effects of switching from modern to LGM dust deposition. a, Modern dust deposition, b, LGM dust deposition, and c, LGM-modern dust deposition difference according to Mahowald et al. (2006); d-i, LGM instead of modern dust deposition rates applied to particle ballasting (LGM_BALL) leading to changes of d, the atmosphere–ocean CO_2 flux (positive into the ocean), e, the common sinking speed $w_{ballast}$ in 100 m depth, f, the organic matter (OM) export in 90 m depth, g, the vertically integrated primary production, h, the calcite export in 90 m depth, and i, the surface dissolved inorganic carbon (DIC) concentration; and j-l, LGM instead of modern dust deposition rates applied to the computation of dust-related iron input (LGM_IRON) leading to changes of j, the atmosphere–ocean CO_2 flux, k, the concentration of diazotrophs, and l, the rain ratio (PIC/POC ratio of the export flux at 90 m depth). The changes are computed from the first 100 years of the sensitivity simulations (LGM_BALL and LGM_IRON) relative to the control simulation with modern dust deposition (~~blue or orange minus black in Fig. 5~~PI_BALLAST).

4.1 Role of LGM dust as ballast

The largest ballasting effect of the LGM dust in our sensitivity experiments occurs in the Southern Ocean off Patagonia. Here, the higher dust deposition rates lead to about 5 to 10 m day^{-1} faster particle sinking in 100 m depth (Fig. 6e), which is equivalent to about a doubling of the sinking speed (compared to Fig. 2~~b~~c). This faster sinking locally leads to a higher export production (Fig. 6f), to a reduced surface dissolved inorganic carbon concentration (Fig. 6i), and consequently to a positive downward net atmosphere–ocean CO_2 flux anomaly (Fig. 6d), which, accumulated over the first ∼3000 years, causes an atmospheric pCO_2 drawdown by about 4.5 ppmv (Fig. 5~~a~~c). This anomalous ocean CO_2 uptake occurs despite a reduction of the globally integrated export production (Fig. 5~~e~~d), as opposed to the locally enhanced export production off Patagonia (Fig. 6f). The smaller globally integrated export production is due to a reduced primary production over wide areas of the Atlantic, Pacific, and Indian Ocean, as well as parts of the Southern Ocean, just north of the area off Patagonia with enhanced organic matter export (Fig. 6g and f). This reduced primary production is consistent with a stronger nitrate depletion in surface waters (not shown) due to increased particle sinking speeds (Fig. 6e). Note that this nitrate depletion can have an effect on primary production globally, since nitrate is the least available nutrient for non-diazotroph phytoplankton everywhere in our model. However, at the same time, the production and export of calcite shells is reduced in the sensitivity simulation (Fig. 6h). Due to higher surface silicate concentrations (not shown), this calcite export reduction is disproportionately large (compared to the POC export reduction), which leads to a reduced rain ratio (Fig. 5~~d~~f). This weakening of the calcium carbonate counter pump overcompensates the effect of the global reduction of the organic matter export on the atmosphere–ocean CO_2 fluxes, leading to a net ocean CO_2 uptake in the first ∼3000 years of our sensitivity experiment.

After about 3000 years, the ocean begins to release CO_2 into the atmosphere again, due to 1) the continuously decreasing export production (Fig. 5d; in response to nitrate depletion), and 2) the slowly recovering calcite production leading to an increasing PIC/POC export ratio anomaly (Fig. 5f).

The observed long-term CO_2 trends may also be affected by interactions with the sediment and by imbalances between sediment burial and weathering fluxes (see, e.g., Ridgwell, 2003). Since the weathering fluxes are the same in all sensitivity experiments (unchanged after the spin-up phase), a rough estimate of the role of sediment interactions can be derived from time series of the total organic carbon and calcite pools in the sediment (not shown). The organic carbon pool in the sediment in the experiment with LGM dust (LGM_BALL) grows faster than in the reference run with modern dust for ballasting (PI_BALLAST), which potentially contributes to the simulated ocean CO_2 uptake. This anomalous organic carbon pool trend amounts to an uptake of about 0.01 Gt C per year by the sediment, which is comparable in magnitude to the atmosphere–ocean CO_2 flux anomalies (Fig. 5b). Moreover, relative to PI_BALLAST, the sediment calcite pool in LGM_BALL is reduced by about $0.2 \cdot 10^{16}$ mol Ca after the first 3000 years of the sensitivity experiment, which can be translated into a global mean ocean alkalinity increase by ∼3 mmol m^{-3}, also potentially contributing to the simulated ∼10 mmol m^{-3} alkalinty increase in LGM_BALL at the surface.

4.2 Role of LGM dust as a source of iron

Iron fertilisation, due to the iron contained in the dust (Section 2.2), also leads to a net CO_2 flux anomaly into the ocean. ~~That~~ In our simulations, this anomalous CO_2 flux ~~is equivalent~~ leads to an atmospheric pCO_2 drawdown by about ~~8~~10 ppmv within ~~4500~~ 6500 years (Fig. 5~~a~~c).

However, as evident from the lack of CO_2 flux anomalies in the Southern Ocean (Fig. 6j), this CO_2 drawdown in our sensitivity experiment is not due to the expected fertilisation of phytoplankton growth by enhanced dust deposition in the Southern Ocean. Hence, the mechanism at work in our iron sensitivity experiment differs from the frequently studied classical iron hypothesis ~~(Martin, 1990; Kumar et al., 1995; Watson et al., 2000; Werner et al., 2002; Bopp et al., 2003; Brovkin et al., 2007; Ganopolski a~~ (Martin, 1990; Kumar et al., 1995; Watson et al., 2000; Werner et al., 2002; Bopp et al., 2003; Brovkin et al., 2007; Martinez-Garcia et al. . The reason for this difference is, that, in contrast to observations (see Boyd et al., 2007, for a review), non-diazotroph phytoplankton growth in our reference simulations (for the standard setup, PI_MARTIN, and the setup with particle ballasting, PI_BALLAST) is limited by nitrate everywhere, and nowhere by iron. Since the diazotroph growth rate, unlike the non-diazotroph phytoplankton growth rate in our model, is not limited by the least available nutrient (Equation 2 of Ilyina et al., 2013), but is proportional to the product of the limiting functions for temperature, iron, phosphate and light (Equations 3 and 8 of Paulsen et al., 2017), the addition of iron can always lead to enhanced diazotroph growth. In fact, we find enhanced diazotroph growth in particular in the tropical Pacific (Fig. 6k), which locally leads to a net positive downward atmosphere–ocean CO_2 flux anomaly (a reduced net CO_2 outgassing in the tropical Pacific; Fig. 6j). This CO_2 flux anomaly is caused by 1) an enhanced organic matter export due to the enhanced diazotroph production (Fig. 5~~e~~d), and 2) the associated reduction of the rain ratio in the tropical Pacific leading to a weakening of the calcium carbonate counter pump (Figs. 5~~d~~ f and 6l). A relative shift from calcifying to silicifying organisms, as reflected by enhanced opal export production (Fig. 5e), also contributes to the weakening of the calcium carbonate counter pump. However, the global mean sinking speed in LGM_IRON hardly differs from that in the reference run with modern dust (PI_BALLAST; Fig. 5a), suggesting that the ballasting effect of the additional opal is balanced by the effect of the reduced calcite export.

Even after 6500 years, the ocean still takes up additional CO_2 from the atmosphere. We attribute most of this long-term trend to a continuously enhanced organic matter export production (Fig. 5d) while the calcite export remains reduced, leading to a continuously lower PIC/POC ratio (Fig. 5f) and to a reduced export of alkalinity. A slightly reduced calcite pool in the sediment in LGM_IRON compared to PI_BALLAST also potentially contributes a small portion to the simulated long term atmospheric pCO_2 drawdown. The sediment calcite pool reduction is equivalent to an alkalinity increase in the water column by less than 2 mmol m^{-3}, compared to a surface alkalinity increase by about 16 mmol m^{-3} after 6500 years in LGM_IRON. Less organic carbon is stored in the sediment in LGM_IRON compared to PI_BALLAST (not shown), which means that the exchange of organic matter between the sediment and the water column does not contribute to the simulated long-term ocean CO_2 uptake in LGM_IRON.

5 Summary and discussion

We estimate the potential effect of aeolian dust deposition changes on glacial–interglacial atmospheric pCO_2 variations by computing the sensitivity of the atmosphere–ocean CO_2 fluxes to LGM dust deposition (Section 4). To this end, we use the ocean circulation and carbon cycle model MPIOM/HAMOCC combined with a new particle ballasting parameterisation (Section 2).

We find that the LGM dust deposition as estimated by Mahowald et al. (2006) leads to faster sinking and enhanced organic matter export off Patagonia, and to a reduction of the calcium carbonate counter pump globally, which results in an anomalous (glacial) ocean CO_2 uptake that is equivalent to an atmospheric pCO_2 drawdown by 4.5 ppmv within 3000 years (Section 4.1).

The iron input associated with the LGM dust deposition causes a fertilisation of diazotroph growth in the tropical Pacific, which leads to an additional atmospheric pCO_2 drawdown by ~~more than 8~~about 10 ppmv within the ~~4000-year-long~~ 6500-year-long sensitivity experiment (Section 4.2). The combination of these effects in response to the LGM dust deposition yields an atmospheric pCO_2 drawdown ~~by about 12 ppmv (~~that is only slightly smaller than the sum of both effects (gray dashed line versus pink line in Fig. 5~~a).~~ c), suggesting that synergistic effects play a minor role here. One negative synergistic effect, for example, which could explain the reduced CO_2 uptake in the combined experiment, is that the additional export production due to diazotroph iron fertilization may be reduced because nutrients are relocated due to particle ballasting.

According to previous modelling studies, iron fertilisation in the Southern Ocean played a large role, leading to an atmospheric pCO_2 drawdown during the LGM by 15-40 ppmv (Watson et al., 2000; Bopp et al., 2003; Brovkin et al., 2007; Lambert et al., 2015; Ganopolski and Brovkin, 2017). However, in our simulations, due to the abundance of iron already for the applied modern dust deposition rates, non-diazotroph phytoplankton production is nowhere iron limited, and the additional iron input associated with the enhanced LGM dust deposition does not lead to a strengthening of the biological pump in the Southern Ocean. ~~It has thus been assumed that~~ This lack of iron limitation could be addressed in future studies for example by reducing the prescribed constant fraction of bio-available iron within the dust in HAMOCC. It is also possible that this lack of iron limitation is due to an overestimation of the modern dust deposition ~~from Mahowald et al. (2006)is an overestimate. Hence~~rates by Mahowald et al. (2006). Both, an older dust depostion estimate by Mahowald et al. (2005) as well as the (to our knowledge) most recent dust deposition estimate by Albani et al. (2016) find (locally in the Southern Ocean and South Atlantic as well as globally) smaller dust deposition rates than suggested by Mahowald et al. (2006). At the HAMOCC development group at the Max-Planck-Institute for Meteorology, since MPIOM revision 4283, which is included in the recent CMIP6-release of MPI-ESM (MPI-ESM version 1.2.01, MPIOM version 1.6.3, revision 4639), the dust deposition fields by Mahowald et al. (2006) were ~~replaced by an~~ therefore replaced by the older dust deposition product ~~(Mahowald et al., 2005) that is characterised by lower dust deposition rates over large areas of the ocean, including the South Atlantic,~~ by Mahowald et al. (2005) again, leading to iron limitation in the Southern Ocean in HAMOCC (Stemmler, personal communication). However, in the model version used here, the dust by Mahowald et al. (2006) is used, and we do not swith back to the older dust deposition field, also because this older version does not provide an estimate of the dust depostion rates during the LGM. The recent estimate by Albani et al. (2016) does provide modern as well as LGM dust deposition estimates,

but this product had not yet been published at the start of this project. The dust estimate by Albani et al. (2016) will be used in future versions of MPIOM/HAMOCC, but the implementation is still ongoing work. We expect that the addition of LGM dust anomalies using a version of MPIOM/HAMOCC that is newer than revision 4283 (using dust fields by Mahowald et al., 2005) or future versions (using dust fields by Albani et al., 2016) will lead to an additional atmospheric pCO_2 drawdown in response to the LGM dust ~~/iron deposition~~ deposition due to the fertilization of non-diazotroph phytoplankton in the Southern Ocean. ~~Therefore, our results likely represent an estimate of the lower bound of the iron effect.~~ This likely explains why the effect of the LGM iron addition on atmospheric pCO_2 is smaller in our simulation than suggested previously. Note that a more realistic iron fertilization response can also lead to modified synergies between iron fertilization and ballasting effects.

~~On the other hand, mesocosm~~ Mesocosm dust deposition experiments in the Mediterranean Sea (Wagener et al., 2010), and their numerical simulation (Ye et al., 2011), as well as more recent simulations of the global iron cycle (Ye and Völker, 2017) indicated that dust can also be a sink for dissolved bio-available iron, because the dust particles provide surfaces for adsorption of dissolved bio-available iron, leading to adsorptive scavenging. By not taking adsorptive scavenging by dust particles into account, we potentially overestimate the effect of dust deposition changes on iron fertilisation.

Aggregate porosity and the degree of aggregate repackaging likely affects sinking speeds, too, as found for example in mesocosm experiments (Bach et al., 2016). In particular, opal ballast during diatom blooms did not lead to higher sinking speeds in the 25 m deep mesocosms, potentially due to the high porosities of the rather fresh aggregates. It is left for future studies to take into account the effect of porosity on the particle sinking speeds in HAMOCC. To avoid the computational expense of explicitly simulating aggregation and the porosities, the fraction of repackaged detritus (by zooplankton) to freshly produced detritus (e.g., by diatoms) could be computed and used to extend the parameterisation of particle sinking speeds.

Also note that no aggregate sizes, size distributions or particle shapes are being computed in our ballasting parameterization, and hence potential effects of aggregate size distribution or shape changes on sinking velocities are neglected (see, e.g., Komar et al., 1981, 1
.

Particle ballasting may play a larger role for glacial–interglacial pCO_2 variations than suggested by the dust-sensitivity alone. Variable ratios of opal/POC or ~~PIC~~calcite/POC can also affect particle sinking speeds via ballasting, and the ratios may have ~~changed in response to, for example,~~ been modified by environmental change, such as variable temperature, variable input of weathering fluxes from land, sea-level or ocean circulation changes. For example, as discussed in Section 3.2, the efficiency of the soft tissue pump in oxygen minimum zones (OMZs) is enhanced due to reduced remineralization rates, but corrosive conditions in OMZs tend to cause reduced calcite concentrations and thereby slower particle sinking speeds, reducing the higher remineralization length scale in OMZs; i.e., the role of oxygenation changes for the soft tissue pump and atmospheric pCO_2 in response to solubility, ocean circulation, or ecosystem variability (e.g., Jaccard and Galbraith, 2012) was potentially modified by particle ballasting. Transient simulations with the coupled MPI-ESM – including, e.g., temperature and ocean circulation changes and their effects on OMZs – are envisaged to quantify the role of these potential additional particle ballasting feedbacks for glacial–interglacial CO_2 variability.

Code and data availability. MPIOM and HAMOCC are available to the scientific community as part of the Max-Planck-Institute Earth System Model MPI-ESM (www.mpimet.mpg.de). Our results are based on MPI-ESM version 1.2.00p4, which includes MPIOM version 1.6.2p3 (corresponding to revision 3997). The modifications to the HAMOCC version 1.6.2p3 source code to include the particle ballasting parameterisation, as well as the model run script to include interactive atmospheric pCO_2 as described in Section 2.2 are provided as supplementary material. To build the model code used in this study, one would need to obtain MPI-ESM via the MPI-ESM-Forum and manually include the code modifications at the described locations. The data to reproduce the figures in this manuscript is available upon request.

Author contributions. All authors were involved in the design of the experiments. M.H. implemented the changes to MPIOM/HAMOCC, carried out the experiments, and wrote the manuscript with support from B.S. and J.S.. B.S. supervised the project.

Competing interests. The authors declare that they have no conflict of interest.

Acknowledgements. The authors thank the Max-Planck-Institute for Meteorology for providing MPI-ESM, and Mathias Heinze, Irene Stemmler and Katharina Six for sharing their HAMOCC expertise. The authors also thank the editor Andrew Yool as well as the three anonymous referees for their constructive comments. The model simulations were performed at the German Climate Computing Centre (DKRZ). This work was supported by the German Federal Ministry of Education and Research (BMBF) as Research for Sustainable Development (FONA, www.fona.de) through the PalMod project (FKZ: 01LP1505D).

References

Abe-Ouchi, A., Segawa, T., and Saito, F.: Climatic Conditions for modelling the Northern Hemisphere ice sheets throughout the ice age cycle, Climate of the Past, 3, 423–438, 2007.

Albani, S., Mahowald, N. M., Murphy, L. N., Raiswell, R., Moore, J. K., Anderson, R. F., McGee, D., Bradtmiller, L. I., Delmonte, B., Hesse, P. P., and Mayewski, P. A.: Paleodust variability since the Last Glacial Maximum and implications for iron inputs to the ocean, Geophysical Research Letters, 43, 3944–3954, 2016.

Anderson, R. F., Barker, S., Fleisher, M., Gersonde, R., Goldstein, S. L., Kuhn, G., Mortyn, P. G., Pahnke, K., and Sachs, J. P.: Biological response to millennial variability of dust and nutrient supply in the Subantarctic South Atlantic Ocean, Philosophical Transactions of the Royal Society A: Mathematical, Physical and Engineering Sciences, 372, 20130 054–20130 054, 2014.

Armstrong, R. A., Lee, C., Hedges, J. I., Honjo, S., and Wakeham, S. G.: A new, mechanistic model for organic carbon fluxes in the ocean based on the quantitative association of POC with ballast minerals, Deep Sea Research Part II: Topical Studies in Oceanography, 49, 219–236, 2002.

Bach, L. T., Boxhammer, T., Larsen, A., Hildebrandt, N., Schulz, K. G., and Riebesell, U.: Influence of plankton community structure on the sinking velocity of marine aggregates, Global Biogeochemical Cycles, 30, 1145–1165, 2016.

Berelson, W. M.: Particle settling rates increase with depth in the ocean, Deep Sea Research Part II: Topical Studies in Oceanography, 49, 237–251, 2001.

Bopp, L., Kohfeld, K. E., Le Quéré, C., and Aumont, O.: Dust impact on marine biota and atmospheric CO_2 during glacial periods, Paleoceanography, 18, 1046, 2003.

Boyd, P. W. and Trull, T. W.: Understanding the export of biogenic particles in oceanic waters: Is there consensus?, Progress in Oceanography, 72, 276–312, 2007.

Boyd, P. W., Jickells, T., Law, C. S., Blain, S., Boyle, E. A., Buesseler, K. O., Coale, K. H., Cullen, J. J., de Baar, H. J. W., Follows, M., Harvey, M., Lancelot, C., Levasseur, M., Owens, N. P. J., Pollard, R., Rivkin, R. B., Sarmiento, J., Schoemann, V., Smetacek, V., Takeda, S., Tsuda, A., Turner, S., and Watson, A. J.: Mesoscale Iron Enrichment Experiments 1993-2005: Synthesis and Future Directions, Science, 315, 612–617, 2007.

Brovkin, V., Ganopolski, A., Archer, D., and Rahmstorf, S.: Lowering of glacial atmospheric CO_2 in response to changes in oceanic circulation and marine biogeochemistry, Paleoceanography, 22, 1–14, 2007.

Brovkin, V., Ganopolski, A., Archer, D., and Munhoven, G.: Glacial CO_2 cycle as a succession of key physical and biogeochemical processes, Climate of the Past, 8, 251–264, 2012.

Bullard, J. E.: Contemporary glacigenic inputs to the dust cycle, Earth Surface Processes and Landforms, 38, 71–89, 2013.

Chikamoto, M. O., Abe-Ouchi, A., Oka, A., Ohgaito, R., and Timmermann, A.: Quantifying the ocean's role in glacial CO_2 reductions, Climate of the Past, 8, 545–563, 2012.

Dunne, J. P., Sarmiento, J. L., and Gnanadesikan, A.: A synthesis of global particle export from the surface ocean and cycling through the ocean interior and on the seafloor, Global Biogeochemical Cycles, 21, 1–16, 2007.

Fischer, G. and Karakaş, G.: Sinking rates and ballast composition of particles in the Atlantic Ocean: implications for the organic carbon fluxes to the deep ocean, Biogeosciences, 2009.

François, R., Honjo, S., Krishfield, R., and Manganini, S.: Factors controlling the flux of organic carbon to the bathypelagic zone of the ocean, Global Biogeochemical Cycles, 16, 34–1–34–20, 2002.

Ganopolski, A. and Brovkin, V.: Simulation of climate, ice sheets and CO_2 evolution during the last four glacial cycles with an Earth system model of intermediate complexity, Climate of the Past, 13, 1695–1716, 2017.

Garcia, E, H., Locarnini, R. A., Boyer, T. P., Antonov, J. I., Baranova, O. K., Zweng, M. M., Reagan, J. R., and Johnson, D. R.: World Ocean Atlas 2013. Vol. 4: Dissolved Inorganic Nutrients (phosphate, nitrate, silicate), NOAA Atlas NESDIS, 76, 25, 2013.

Gehlen, M., Bopp, L., Emprin, N., Aumont, O., Heinze, C., and O, R.: Reconciling surface ocean productivity, export fluxes and sediment composition in a global biogeochemical ocean model, Biogeosciences, 3, 521–537, 2006.

Giorgetta, M. A., Jungclaus, J., Reick, C. H., Legutke, S., Bader, J., Böttinger, M., Brovkin, V., Crueger, T., Esch, M., Fieg, K., Glushak, K., Gayler, V., Haak, H., Hollweg, H.-D., Ilyina, T., Kinne, S., Kornblueh, L., Matei, D., Mauritsen, T., Mikolajewicz, U., Mueller, W., Notz, D., Pithan, F., Raddatz, T., Rast, S., Redler, R., Roeckner, E., Schmidt, H., Schnur, R., Segschneider, J., Six, K. D., Stockhause, M., Timmreck, C., Wegner, J., Widmann, H., Wieners, K.-H., Claussen, M., Marotzke, J., and Stevens, B.: Climate and carbon cycle changes from 1850 to 2100 in MPI-ESM simulations for the Coupled Model Intercomparison Project phase 5, Journal of Advances in Modeling Earth Systems, 5, 572–597, 2013.

Hain, M. P., Sigman, D. M., and Haug, G. H.: Carbon dioxide effects of Antarctic stratification, North Atlantic Intermediate Water formation, and subantarctic nutrient drawdown during the last ice age: Diagnosis and synthesis in a geochemical box model, Global Biogeochemical Cycles, 24, n/a–n/a, 2010.

Heinemann, M., Timmermann, A., Elison Timm, O., Saito, F., and Abe-Ouchi, A.: Deglacial ice sheet meltdown: orbital pacemaking and CO_2 effects, Climate of the Past, 10, 1567–1579, 2014.

Heinze, C., Reimer, E. M., Winguth, A. M. E., and Archer, D.: A global oceanic sediment model for long-term climate studies, Global Biogeochemical Cycles, 13, 221–250, 1999.

Henson, S. A., Sanders, R., and Madsen, E.: Global patterns in efficiency of particulate organic carbon export and transfer to the deep ocean, Global Biogeochemical Cycles, 26, GB1028, 2012.

Hofmann, M. and Schellnhuber, H.-J.: Oceanic acidification affects marine carbon pump and triggers extended marine oxygen holes, PNAS, 106, 3017–3022, 2009.

Honjo, S., Manganini, S. J., and Cole, J. J.: Sedimentation of biogenic matter in the deep ocean, Deep-Sea Research, 29, 609–625, 1982.

Honjo, S., Manganini, S. J., Krishfield, R. A., and François, R.: Particulate organic carbon fluxes to the ocean interior and factors controlling the biological pump: A synthesis of global sediment trap programs since 1983, Progress in Oceanography, 76, 217–285, 2008.

Howard, M. T., Winguth, A. M. E., Klaas, C., and Reimer, E. M.: Sensitivity of ocean carbon tracer distributions to particulate organic flux parameterizations, Global Biogeochemical Cycles, 20, 1–11, 2006.

Ilyina, T., Six, K. D., Segschneider, J., Maier-Reimer, E., Li, H., and Núñez-Riboni, I.: Global ocean biogeochemistry model HAMOCC: Model architecture and performance as component of the MPI-Earth system model in different CMIP5 experimental realizations, Journal of Advances in Modeling Earth Systems, 5, 287–315, 2013.

Ittekkot, V.: The abiotically driven biological pump in the ocean and short-term fluctuations in atmospheric CO_2 contents, Global and Planetary Change, 8, 17–25, 1993.

Jaccard, S. L. and Galbraith, E. D.: Large climate-driven changes of oceanic oxygen concentrations during the last deglaciation, Nature Geoscience, 5, 151–156, 2012.

Jungclaus, J. H., Lorenz, S. J., Timmreck, C., Reick, C. H., Brovkin, V., Six, K., Segschneider, J., Giorgetta, M. A., Crowley, T. J., Pongratz, J., Krivova, N. A., Vieira, L. E., Solanki, S. K., Klocke, D., Botzet, M., Esch, M., Gayler, V., Haak, H., Raddatz, T. J., Roeckner, E.,

Schnur, R., Widmann, H., Claussen, M., Stevens, B., and Marotzke, J.: Climate and carbon-cycle variability over the last millennium, Climate of the Past, 6, 723–737, 2010.

Jungclaus, J. H., Fischer, N., Haak, H., Lohmann, K., Marotzke, J., Matei, D., Mikolajewicz, U., Notz, D., and von Storch, J. S.: Characteristics of the ocean simulations in the Max Planck Institute Ocean Model (MPIOM) the ocean component of the MPI-Earth system model, Journal of Advances in Modeling Earth Systems, 5, 422–446, 2013.

Klaas, C. and Archer, D. E.: Association of sinking organic matter with various types of mineral ballast in the deep sea: Implications for the rain ratio, Global Biogeochemical Cycles, 16, 2002.

Köhler, P., Nehrbass-Ahles, C., Schmitt, J., Stocker, T. F., and Fischer, H.: A 156 kyr smoothed history of the atmospheric greenhouse gases CO_2, CH_4, and N_2O and their radiative forcing, Earth System Science Data, 9, 363–387, 2017.

Komar, P. D., Morse, A. P., Small, L. F., and Fowler, S. W.: An analysis of sinking rates of natural copepod and euphausiid fecal pellets1, Limnology and Oceanography, 26, 172–180, 1981.

Kriest, I. and Evans, G. T.: A vertically resolved model for phytoplankton aggregation, Journal of Earth System Science, 109, 453–469, 2000.

Kumar, N., Anderson, R. F., Mortlock, R. A., Froelich, P. N., Kubik, P., Dittrich-Hannen, B., and Suter, M.: Increased biological productivity and export production in the glacial Southern Ocean, Nature, 378, 675–680, 1995.

Lam, P. J. and Marchal, O.: Insights into Particle Cycling from Thorium and Particle Data, Annual Review of Marine Science, 7, 159–184, 2015.

Lambert, F., Tagliabue, A., Shaffer, G., Lamy, F., Winckler, G., Farias, L., Gallardo, L., and De Pol-Holz, R.: Dust fluxes and iron fertilization in Holocene and Last Glacial Maximum climates, Geophysical Research Letters, 42, 6014–6023, 2015.

Lüthi, D., Le Floch, M., Bereiter, B., Blunier, T., Barnola, J.-M., Siegenthaler, U., Raynaud, D., Jouzel, J., Fischer, H., Kawamura, K., and Stocker, T. F.: High-resolution carbon dioxide concentration record 650,000-800,000 years before present, Nature, 453, 379–382, 2008.

Mahowald, N. M., Baker, A. R., Bergametti, G., Brooks, N., Duce, R. A., Jickells, T. D., Kubilay, N., Prospero, J. M., and Tegen, I.: Atmospheric global dust cycle and iron inputs to the ocean, Global Biogeochemical Cycles, 19, GB4025, 2005.

Mahowald, N. M., Muhs, D. R., Levis, S., Rasch, P. J., Yoshioka, M., Zender, C. S., and Luo, C.: Change in atmospheric mineral aerosols in response to climate: Last glacial period, preindustrial, modern, and doubled carbon dioxide climates, Journal of Geophysical Research: Solid Earth, 111, 2006.

Maier-Reimer, E., Kriest, I., Segschneider, J., and Wetzel, P.: The HAMburg Ocean Carbon Cycle Model HAMOCC5.1 - Technical Description Release 1.1, Berichte zur Erdsystemforschung, 14, 2005.

Marcott, S. A., Bauska, T. K., Buizert, C., Steig, E. J., Rosen, J. L., Cuffey, K. M., Fudge, T. J., Severinghaus, J. P., Ahn, J., Kalk, M. L., McConnell, J. R., Sowers, T., Taylor, K. C., White, J. W. C., and Brook, E. J.: Centennial-scale changes in the global carbon cycle during the last deglaciation, Nature, 514, 616–619, 2014.

Marsland, S. J., Haak, H., Jungclaus, J. H., Latif, M., and Röske, F.: The Max-Planck-Institute global ocean/sea ice model with orthogonal curvilinear coordinates, Ocean Modelling, 5, 91–127, 2003.

Martin, J. H.: Glacial-interglacial CO_2 change: The Iron Hypothesis, Paleoceanography, 5, 1–13, 1990.

Martin, J. H., Knauer, G. A., Karl, D. M., and Broenkow, W. W.: VERTEX: carbon cycling in the northeast Pacific, Deep Sea Research Part A. Oceanographic Research Papers, 34, 267–285, 1987.

Martinez-Garcia, A., Sigman, D. M., Ren, H., Anderson, R. F., Straub, M., Hodell, D. A., Jaccard, S. L., Eglinton, T. I., and Haug, G. H.: Iron Fertilization of the Subantarctic Ocean During the Last Ice Age, Science, 343, 1347–1350, 2014.

Paulsen, H., Ilyina, T., Six, K. D., and Stemmler, I.: Incorporating a prognostic representation of marine nitrogen fixers into the global ocean biogeochemical model HAMOCC, Journal of Advances in Modeling Earth Systems, 2017.

Raddatz, T. J., Reick, C. H., Knorr, W., Kattge, J., Roeckner, E., Schnur, R., Schnitzler, K. G., Wetzel, P., and Jungclaus, J.: Will the tropical land biosphere dominate the climate–carbon cycle feedback during the twenty-first century?, Climate Dynamics, 29, 565–574, 2007.

Ridgwell, A. J.: An end to the "rain ratio" reign?, Geochemistry Geophysics Geosystems, 4, 1–5, 2003.

Röske, F.: Global oceanic heat and fresh water forcing datasets based on ERA-40 and ERA-15, Berichte zur Erdsystemforschung, 13, 2005.

Röske, F.: A global heat and freshwater forcing dataset for ocean models, Ocean Modelling, 11, 235–297, 2006.

Sigman, D. M. and Boyle, E. A.: Glacial/interglacial variations in atmospheric carbon dioxide, Nature, 407, 859–869, 2000.

Stevens, B., Giorgetta, M., Esch, M., Mauritsen, T., Crueger, T., Rast, S., Salzmann, M., Schmidt, H., Bader, J., Block, K., Brokopf, R., Fast, I., Kinne, S., Kornblueh, L., Lohmann, U., Pincus, R., Reichler, T., and Roeckner, E.: Atmosphere component of the MPI-M Earth System Model: ECHAM6, Journal of Advances in Modeling Earth Systems, 5, 146–172, 2013.

Takahashi, T., Sutherland, S. C., Wanninkhof, R., Sweeney, C., Feely, R. A., Chipman, D. W., Hales, B., Friederich, G., Chavez, F., Sabine, C., Watson, A., Bakker, D. C. E., Schuster, U., Metzl, N., Yoshikawa-Inoue, H., Ishiik, M., Midorikawak, T., Nojiril, Y., Körtzinger, A., Tobias Steinhoffm, M. H. n., Hoppema, M., Olafsson, J., Arnarson, T. S., Tilbrook, B., Johannessen, T., Olsen, A., Bellerby, R., Wong, C. S., Delille, B., Bates, N. R., and de Baar, H. J. W.: Climatological mean and decadal change in surface ocean pCO_2, and net sea–air CO_2 flux over the global oceans, Deep-Sea Research II, 56, 554–577, 2009.

van der Jagt, H., Friese, C., Stuut, J. B. W., Fischer, G., and Iversen, M. H.: The ballasting effect of Saharan dust deposition on aggregate dynamics and carbon export: Aggregation, settling, and scavenging potential of marine snow, Limnology and Oceanography, 63, 1386–1394, 2018.

Wagener, T., Guieu, C., and Leblond, N.: Effects of dust deposition on iron cycle in the surface Mediterranean Sea: results from a mesocosm seeding experiment, Biogeosciences, 7, 3769–3781, 2010.

Watson, A. J., Bakker, D. C. E., Ridgwell, A. J., Boyd, P. W., and Law, C. S.: Effect of iron supply on Southern Ocean CO_2 uptake and implications for glacial atmospheric CO_2, Nature, 407, 730–733, 2000.

Weber, T., Cram, J. A., and Leung, S. W.: Deep ocean nutrients imply large latitudinal variation in particle transfer efficiency, PNAS, 113, 8606–8611, 2016.

Werner, M., Tegen, I., Harrison, S. P., Kohfeld, K. E., Prentice, I. C., Balkanski, Y., Rodhe, H., and Roelandt, C.: Seasonal and interannual variability of the mineral dust cycle under present and glacial climate conditions, Journal of Geophysical Research, 107, 4744, 2002.

Wetzel, P., Maier-Reimer, E., Botzet, M., Jungclaus, J., Keenlyside, N., and Latif, M.: Effects of Ocean Biology on the Penetrative Radiation in a Coupled Climate Model, Journal of Climate, 19, 3973–3987, 2006.

Ye, Y. and Völker, C.: On the Role of Dust-Deposited Lithogenic Particles for Iron Cycling in the Tropical and Subtropical Atlantic, Global Biogeochemical Cycles, 31, 1543–1558, 2017.

Ye, Y., Wagener, T., Völker, C., Guieu, C., and Wolf-Gladrow, D. A.: Dust deposition: iron source or sink? A case study, Biogeosciences, 8, 2107–2124, 2011.